



TITLE:

Nonlinear mechanisms of lower-band and upper-band VLF chorus emissions in the magnetosphere

AUTHOR(S):

Omura, Yoshiharu; Hikishima, Mitsuru; Katoh, Yuto; Summers, Danny; Yagitani, Satoshi

CITATION:

Omura, Yoshiharu ...[et al]. Nonlinear mechanisms of lower-band and upper-band VLF chorus emissions in the magnetosphere. Journal of Geophysical Research A: Space Physics 2009, 114(7): A07217.

ISSUE DATE:

2009

URL:

<http://hdl.handle.net/2433/91257>

RIGHT:

An edited version of this paper was published by AGU. Copyright (2009) American Geophysical Union.; This is not the published version. Please cite only the published version.; この論文は出版社版ではありません。引用の際には出版社版をご確認ご利用ください。

Nonlinear mechanisms of lower band and upper band VLF chorus emissions in the magnetosphere

Yoshiharu Omura,¹ Mitsuru Hikishima,^{1,2} Yuto Katoh,^{1,3}

Danny Summers,^{1,4,5} and Satoshi Yagitani²

¹ Research Institute for Sustainable Humanosphere, Kyoto University, Kyoto Japan.

²
Kanazawa University, Kanazawa, Japan.

³ Planetary Plasma and Atmospheric Research Center, Graduate School of Science, Tohoku
University, Miyagi, Japan.

⁴ Department of Mathematics and Statistics, Memorial University of Newfoundland, St. John's,
Newfoundland, Canada.

⁵ School of Space Research, Kyung Hee University, Yongin, Gyeonggi, Korea.

Yoshiharu Omura, Research Institute for Sustainable Humanosphere, Kyoto University, Uji,
Kyoto, 611-0011, Japan. (omura@rish.kyoto-u.ac.jp)

Mitsuru Hikishima, Research Institute for Sustainable Humanosphere, Kyoto University, Uji,

chorus emissions, taking into account the spatial inhomogeneity of the static magnetic field and the plasma density variation along the magnetic field line. We derive theoretical expressions for the nonlinear growth rate and the amplitude threshold for the generation of self-sustaining chorus emissions. We assume that nonlinear growth of a whistler-mode wave is initiated at the magnetic equator where the linear growth rate maximizes. Self-sustaining emissions become possible when the wave propagates away from the equator during which process the increasing gradients of the static magnetic field and electron density provide the conditions for nonlinear growth. The amplitude threshold is tested against both observational data and self-consistent particle simulations of the chorus emissions. The self-sustaining mechanism can result in a rising tone emission covering the frequency range of $0.1 - 0.7 \Omega_{e0}$ where Ω_{e0} is the equatorial electron gyrofrequency. During propagation higher frequencies are subject to stronger dispersion effects that can destroy the self-

Kyoto, 611-0011, Japan. (hikishima@rish.kyoto-u.ac.jp)

Yuto Katoh, Planetary Plasma and Atmospheric Research Center, Graduate School of Science, Tohoku University, 980-8578, Miyagi, Japan. (yuto@pparc.geophys.tohoku.ac.jp)

Danny Summers, Department of Mathematics and Statistics, Memorial University of Newfoundland, St. John's, Newfoundland, A1C 5S7, Canada. (dsummers@math.mun.ca)

Satoshi Yagitani, Graduate School of Natural Science and Technology, Kanazawa University, Kakuma, Kanazawa 920-1192, Japan. (yagitani@is.t.kanazawa-u.ac.jp)

growing mechanism. We obtain a pair of coupled differential equations for

the wave amplitude and frequency. Solving the equations numerically, we re-
produce a rising tone of VLF whistler-mode emissions that is continuous in
frequency. Chorus emissions, however, characteristically occur in two distinct
frequency ranges, a lower band and an upper band, separated at half the elec-
tron gyrofrequency. We explain the gap by means of the nonlinear damping
of the longitudinal component of a slightly oblique whistler-mode wave packet
propagating along the inhomogeneous static magnetic field.

1. Introduction

Coherent electromagnetic waves called chorus emissions have been frequently observed in the inner magnetosphere [e.g., *Tsurutani and Smith*, 1974; *Anderson and Kurth*, 1989; *Lauben et al.*, 1998, 2002; *Santolik et al.*, 2003; *Santolik*, 2008; *Kasashara et al.*, 2009]. Chorus emissions typically consist of a series of rising tones near the magnetic equator, excited by energetic electrons from several keV to tens of keV injected into the inner magnetosphere at the time of a geomagnetic disturbance. In recent years chorus emissions have been studied extensively because of their role as a viable mechanism for accelerating radiation belt electrons [*Summers et al.*, 1998, 2002, 2004a,b, 2007a,b; *Roth et al.*, 1999; *Summers and Ma*, 2000; *Albert*, 2000, 2002; *Miyoshi et al.*, 2003; *Horne et al.*, 2005; *Omura et al.*, 2007; *Katoh and Omura*, 2004, 2007a; *Summers and Omura*, 2007; *Furuya et al.*, 2008; *Katoh et al.*, 2008]

Numerical modeling of chorus emissions have been performed using a Vlasov-hybrid simulation based on simplified field equations derived from Maxwell's equations under the assumption of a coherent whistler-mode wave [*Nunn*, 1974; *Nunn et al.*, 1997]. The initial wave amplitude and the wave phase are specified in such simulations. In contrast to the Vlasov-hybrid simulation, chorus emissions with rising tones were reproduced successfully in an electron-hybrid electromagnetic code starting from thermal noise. Here, Maxwell's equations are solved directly together with the electron fluid equation for the cold dense electrons and the equations of motion for the hot resonant electrons [*Katoh and Omura*, 2006; 2007b]. The mechanism of the rising chorus emissions has been analyzed theoretically in terms of nonlinear wave growth due to the formation of an electromag-

electron hole in velocity phase space [Omura *et al.*, 2008]. The relation between the

wave amplitude and the frequency sweep rate in the generation region of chorus emissions has been derived [Omura *et al.*, 2008, Equation (50)]. The validity of this relation has been demonstrated in a full-particle electromagnetic simulation [Hikishima *et al.*, 2009] as well as in the electron-hybrid simulation [Kato and Omura, 2007b]. These simulations show that seeds of chorus emissions with rising tones are formed in a localized region near the magnetic equator. The seeds of emissions grow as a result of the formation of a resonant current arising from nonlinear trajectories of resonant untrapped electrons. The generation mechanism [Omura *et al.*, 2008] is clearly different from those proposed in the previous studies [Nunn *et al.*, 1997; Trakhtengerts *et al.*, 1995; 1999] which assume that the frequency variation of chorus emissions is driven by an out-of-phase resonant current.

We first derive the nonlinear wave growth rate in section 2 based on nonlinear trajectories of resonant electrons interacting with a whistler-mode wave with a variable frequency. This is an extension of the theoretical analysis of an electromagnetic electron hole by Omura *et al.* [2008]. The key element in the derivation of the nonlinear growth rate is the frequency sweep rate of the growing chorus element near the equator. In section 3, we study the dispersion effect that modifies the frequency sweep rate during propagation due to the frequency dependence of the group velocity. The nonlinear growth is sustained over a relatively long distance of propagation by the inhomogeneity of the dipole magnetic field. In section 4 we obtain an amplitude threshold from the condition of the absolute instability at the magnetic equator. When the wave amplitude exceeds the threshold the wave amplitude grows along with the increasing frequency. In section 5 we derive a pair of coupled differential equations for the wave amplitude and the frequency which we call

rus equations”. These equations reproduce the characteristic features of a rising chorus element. We solve them numerically with parameters used in the recent simulations by *Katoh and Omura* [2007b] and *Hikishima et al.* [2009]. We find excellent agreement between the simulations and the solutions of the chorus equations. Most of the rising tone emissions starting from a frequency lower than half the gyrofrequency terminate just below half the gyrofrequency. This obviously suggests a possible damping mechanism of rising tone emissions occurring at half the gyrofrequency. Herein we propose a new mechanism to explain whistler-mode wave damping at half the gyrofrequency which we present in section 6. In section 7, we solve the chorus equations using two sets of parameters, namely for the Earth’s magnetosphere [*Santolik et al.*, 2003] and Saturn’s magnetosphere [*Hospodarsky et al.*, 2008]. We find that the duration times of chorus emissions are much different for Earth and Saturn. In section 8 we present the summary and discussion.

2. Nonlinear growth rate

We assume a coherent electromagnetic wave propagating parallel to a static magnetic field \mathbf{B}_0 directed along the h -axis, and h is the distance along the magnetic field line from the magnetic equator. The wave fields are in the transverse plane containing x - and y -axes. We express the electric and magnetic field vectors of the wave in the transverse plane by the complex forms $\tilde{E}_w = E_w \exp(i\psi_E)$ and $\tilde{B}_w = B_w \exp(i\psi_B)$, respectively. From Maxwell’s equations we obtain the following equation for the amplitude B_w of the wave magnetic field in the form [*Omura et al.*, 2008],

$$\frac{\partial B_w}{\partial t} + V_g \frac{\partial B_w}{\partial h} = -\frac{\mu_0 V_g}{2} J_E \quad , \quad (1)$$

μ_0 and J_E are the vacuum permeability and the component of the resonant current

parallel to the wave electric field, respectively. Under the assumption that the growth rate ω_i is much smaller than the wave frequency ω , i.e., $\omega_i \ll \omega$, the resonant current parallel to the wave magnetic field J_B is neglected. This ensures that the frequency ω is constant in the frame of reference moving with the group velocity V_g as expressed by the equation,

$$\frac{\partial \omega}{\partial t} + V_g \frac{\partial \omega}{\partial h} = 0 \quad . \quad (2)$$

The frequency ω and wave number k satisfy the cold plasma dispersion relation for the whistler-mode wave which we write as

$$\delta^2 = \frac{1}{1 + \xi^2} \quad , \quad (3)$$

where δ and ξ are dimensionless parameters defined by

$$\delta^2 = 1 - \frac{\omega^2}{c^2 k^2} \quad (4)$$

and

$$\xi^2 = \frac{\omega(\Omega_e - \omega)}{\omega_{pe}^2} \quad . \quad (5)$$

These parameters are determined by the speed of light c , electron plasma frequency ω_{pe} , and electron gyrofrequency Ω_e as shown above.

Using these parameters, we express the phase velocity and group velocity of the whistler-mode wave as [Omura *et al.*, 2008]

$$V_p = \frac{\omega}{k} = c\delta\xi \quad (6)$$

and

$$V_g = \frac{c\xi}{\delta} \left[\xi^2 + \frac{\Omega_e}{2(\Omega_e - \omega)} \right]^{-1} \quad . \quad (7)$$

electron resonance velocity for an electron with a speed v is then

$$V_R = c\delta\xi \left(1 - \frac{\Omega_e}{\gamma\omega}\right) , \quad (8)$$

where γ is the Lorentz factor given by $\gamma = [1 - (v/c)^2]^{-1/2}$. Using the relativistic equations of motion for a resonant electron interacting with a whistler-mode wave [Omura *et al.*, 2008], we obtain the second-order nonlinear ordinary differential equation for the phase angle ζ ,

$$\frac{d^2\zeta}{dt^2} = \frac{\omega_t^2 \delta^2}{\gamma} (\sin \zeta + S) , \quad (9)$$

where ω_t is the trapping frequency given by $\omega_t = \sqrt{kV_{\perp 0}\Omega_w}$ [Matsumoto and Omura, 1981; Omura and Matsumoto, 1982]. The parameters $V_{\perp 0}$ and Ω_w are the average perpendicular velocity and the normalized wave amplitude defined by $\Omega_w = eB_w/m_0$, where $-e$ and m_0 are the charge and rest mass of an electron. The parameter S is the inhomogeneity ratio given by

$$S = -\frac{1}{s_0\omega\Omega_w} \left(s_1 \frac{\partial\omega}{\partial t} + cs_2 \frac{\partial\Omega_e}{\partial h} \right) , \quad (10)$$

where

$$s_0 = \frac{\delta}{\xi} \frac{V_{\perp 0}}{c} , \quad (11)$$

$$s_1 = \gamma \left(1 - \frac{V_R}{V_g}\right)^2 , \quad (12)$$

and

$$s_2 = \frac{1}{2\xi\delta} \left\{ \frac{\gamma\omega}{\Omega_e} \left(\frac{V_{\perp 0}}{c} \right)^2 - \left[2 + \Lambda \frac{\delta^2(\Omega_e - \gamma\omega)}{\Omega_e - \omega} \right] \frac{V_R V_p}{c^2} \right\} , \quad (13)$$

and we have introduced the parameter Λ . We have incorporated the variation of the cold electron density $N_e(h)$ along the magnetic field line as $N_e(h) = N_{e0}\Omega_e(h)/\Omega_{e0}$, where N_{e0}

Ω_{e0} are respectively the cold electron density and the electron gyrofrequency at the

equator. We find that $\Lambda = \omega/\Omega_e$ for this inhomogeneous electron density model (see Appendix A), while $\Lambda = 1$ for the constant electron density model as assumed by *Omura et al.* [2008]. In the slow-wave approximation, we set $\delta = 1$ and $\gamma = 1$ in (9) - (13) and so obtain simplified equations for the resonant particles [*Omura et al.*, 1991].

From the analysis of trajectories of resonant electrons as described by (9), it is found that the maximum value of J_E is realized when $S = -0.4$ [Omura *et al.*, 2008]. The magnitude of J_E is calculated by assuming a distribution function in the velocity phase space in the presence of a coherent whistler-mode wave as

$$g(v_{\parallel}, \zeta) = g_0(v_{\parallel}) - Qg_t(v_{\parallel}, \zeta) \quad , \quad (14)$$

and we have

$$J_E = -eQV_{\perp 0}^2 \int_0^{2\pi} \int_{-\infty}^{\infty} g_t(v_{\parallel}, \zeta) \sin \zeta dv_{\parallel} d\zeta \quad , \quad (15)$$

where we have assumed a Dirac delta function $\Delta(v_{\perp} - V_{\perp 0})$ for the perpendicular velocity v_{\perp} . The functions $g_0(v_{\parallel})$ and $g_t(v_{\parallel}, \zeta)$ are the unperturbed velocity distribution function and the part of g_0 that corresponds to trapping by the wave. Since the separatrix of the trapping wave potential is closed, the entrapping of new particles does not take place unless the wave amplitude increases. At this stage there arises an electron hole in the velocity phase space [Omura and Summers, 2006]. We assume that the factor Q represents the depth of the electron hole. If $Q = 1$ the electron hole is completely void. If 50 % of trapped electrons are lost from the trapping wave potential, then $Q = 0.5$. Assuming that $g_t(v_{\parallel}, \zeta) = G$ ($= \text{constant}$) inside the trapping region and $g_t(v_{\parallel}, \zeta) = 0$ outside it,

$$J_E = -J_0 \int_{\zeta_1}^{\zeta_2} [\cos \zeta_1 - \cos \zeta + S(\zeta - \zeta_1)]^{1/2} \sin \zeta d\zeta \quad , \quad (16)$$

where $J_0 = (2e)^{3/2} (m_0 k \gamma)^{-1/2} V_{\perp 0}^{5/2} \delta Q G B_w^{1/2}$, and e and m_0 are the charge and rest mass of an electron. The phase angles ζ_1 and ζ_2 define the boundary of the trapping wave potential as described by *Omura et al.* [2008]. The current $-J_E$ is a function of S and maximizes at $S = -0.4$. The maximum value is given by $-J_E/J_0 = 0.975 \sim 1$. We thus have

$$J_{E,max} = -(2e)^{3/2} (m_0 k \gamma)^{-1/2} V_{\perp 0}^{5/2} B_w^{1/2} Q G \delta \quad . \quad (17)$$

Writing the right-hand side of (1) as dB_w/dt , we obtain

$$\frac{dB_w}{dt} = \frac{\mu_0 V_g}{2} (2e)^{3/2} \left(\frac{c \xi \delta}{m_0 \omega \gamma} \right)^{1/2} V_{\perp 0}^{5/2} B_w^{1/2} Q G \delta \quad , \quad (18)$$

where we have eliminated the wave number k using (6). We assume that the velocity distribution function f of hot energetic electrons is given in terms of the relativistic momentum per unit mass $u = \gamma v$; u has components $u_{\parallel} = \gamma v_{\parallel}$ and $u_{\perp} = \gamma v_{\perp}$, respectively parallel and perpendicular to the ambient magnetic field. We specify f as

$$f(u_{\parallel}, u_{\perp}) = \frac{N_h}{(2\pi)^{3/2} U_{t\parallel} U_{\perp 0}} \exp \left(-\frac{u_{\parallel}^2}{2U_{t\parallel}^2} \right) \Delta(u_{\perp} - U_{\perp 0}) \quad , \quad (19)$$

where $U_{\perp 0} = \gamma V_{\perp 0}$, and Δ is the Dirac delta function, and we have normalized f to the density of hot electrons N_h . Integrating over u_{\perp} and taking an average over ζ , we obtain the magnitude G of the unperturbed distribution function $g(v_{\parallel}, \zeta)$ at the resonance velocity V_R as

$$G = \frac{N_h}{(2\pi)^{3/2} U_{t\parallel} U_{\perp 0}} \exp \left(-\frac{\gamma^2 V_R^2}{2U_{t\parallel}^2} \right) \quad . \quad (20)$$

binning (18) and (20), we obtain the result,

$$\frac{dB_w}{dt} = \Gamma_N B_w, \quad (21)$$

where we define

$$\Gamma_N = \frac{Q\omega_{ph}^2}{2} \left(\frac{\xi}{\Omega_w \omega} \right)^{1/2} \frac{V_g}{U_{t\parallel}} \left(\frac{V_{\perp 0} \delta}{c\pi\gamma} \right)^{3/2} \exp \left(-\frac{\gamma^2 V_R^2}{2U_{t\parallel}^2} \right) \quad (22)$$

as the nonlinear growth rate. The parameter ω_{ph} is the plasma frequency of hot electrons given by $\omega_{ph}^2 = N_h e^2 / (\epsilon_0 m_0)$, where ϵ_0 is the vacuum permittivity. It should be noted that we have defined Γ_N as the nonlinear wave growth rate by analogy with the linear growth rate. In Figure 1, we plot Γ_N for the indicated set of parameters and the plasma frequencies $\omega_{pe} = 2, 4, 8, 16 \Omega_{e0}$. The nonlinear growth rate maximizes in the lower band $0 < \omega/\Omega_{e0} < 0.5$ for plasma frequencies $\omega_{pe}/\Omega_{e0} \geq 3$, and maximizes in the upper band $0.5 < \omega/\Omega_{e0} < 1.0$ when $\omega_{pe}/\Omega_{e0} \leq 2$.

3. Spatial variation of the frequency sweep rate

As we have seen in the previous section, the nonlinear growth of a chorus element near the equator is controlled by the frequency sweep rate or the time derivative of the frequency $\partial\omega/\partial t$. We consider here how the frequency sweep rate evolves in space during the wave propagation. We assume that a chorus element is excited at the equator ($h = 0$). The propagation of the wave frequency is described by equation (2). We consider the motion of two segments of a chorus element with frequencies ω_1 and ω_2 (with $\omega_1 < \omega_2$) and group velocities V_{g1} and V_{g2} , respectively, schematically illustrated in Figure 2. We assume that the segments with frequencies ω_1 and ω_2 are generated at the equator at times $t = 0$ and

$$\omega_2 = \omega_1 + \left(\frac{\partial \omega}{\partial t} \right)_{t=0} \Delta t . \quad (23)$$

Taking the group velocity as constant in space, we find that after the chorus element propagates for a period of T the segment with frequency ω_1 reaches the location $h_1 = V_{g1}(\Delta t + T)$, while the segment with frequency ω_2 reaches $h_2 = V_{g2}T$.

Since the group velocity is a function of ω , we have

$$V_{g2} = V_{g1} + \left(\frac{\partial V_g}{\partial \omega} \frac{\partial \omega}{\partial t} \right)_{t=0} \Delta t . \quad (24)$$

We calculate the spatial gradient of the frequency at $t = T$ as

$$\left(\frac{\partial \omega}{\partial h} \right)_{t=T} = \lim_{\Delta t \rightarrow 0} \frac{\omega_1 - \omega_2}{h_1 - h_2} = \frac{-(\partial \omega / \partial t)_{t=0}}{V_{g1} - T(\partial V_g / \partial \omega)(\partial \omega / \partial t)_{t=0}} . \quad (25)$$

Using equation (2), and assuming that the chorus element generated at $t = 0$ and $h = 0$ propagates a distance h_T over the period T , i.e., $h_T = V_g T$, we obtain the relation,

$$\left(\frac{\partial \omega}{\partial t} \right)_{h=h_T} = \left[1 - \frac{h_T}{V_g^2} \frac{\partial V_g}{\partial \omega} \left(\frac{\partial \omega}{\partial t} \right)_{h=0} \right]^{-1} \left(\frac{\partial \omega}{\partial t} \right)_{h=0} . \quad (26)$$

Using equation (7) for V_g , we calculate its derivative in Appendix B as

$$\frac{\partial V_g}{\partial \omega} = \frac{V_g^2 \delta^3}{4c\xi\omega(\Omega_e - \omega)^2} \left[\Omega_e - 2\omega(1 - \frac{1}{\delta}) \right] \left[\Omega_e - 2\omega(1 + \frac{1}{\delta}) \right] . \quad (27)$$

It follows from equation (27) that the frequency at which V_g maximizes is

$$\omega = \frac{\Omega_e}{2(1 + 1/\delta)} . \quad (28)$$

For $\omega_{pe} \gg \Omega_e$, $\delta \sim 1$, and thus V_g maximizes at $\omega \sim 0.25\Omega_e$, as shown in Figure 3(a).

Substituting (27) into (26), we obtain

$$\left(\frac{\partial \omega}{\partial t} \right)_{h=h_T} = D \left(\frac{\partial \omega}{\partial t} \right)_{h=0} , \quad (29)$$

$$D = \left[1 - \frac{\delta^3(\Omega_e^2 - 4\omega\Omega_e - 4\xi^2\omega^2)}{4c\xi\omega(\Omega_e - \omega)^2} h_T \left(\frac{\partial\omega}{\partial t} \right)_{h=0} \right]^{-1} . \quad (30)$$

We plot D for the cases $h_T(\partial\omega/\partial t)_{h=0} = 0.0001, 0.001, 0.01, 0.05 c\Omega_{e0}$ in Figure 3(b). We see that the frequency sweep rate factor D can remain nearly constant over the frequency range $0.1 \sim 0.7 \Omega_{e0}$ in spite of the variation of the group velocity and the phase velocity with respect to frequency ω so long as $h_T(\partial\omega/\partial t)_{h=0} \leq 0.001 c\Omega_{e0}$.

4. Threshold for self-sustaining emissions

We derive a necessary condition for a chorus element to be amplified during propagation from the equator to a higher latitude region. Expressing the derivative dB_w/dt in (21) in terms of temporal and spatial derivatives and normalizing the wave amplitude, we obtain

$$\frac{\partial\Omega_w}{\partial t} + V_g \frac{\partial\Omega_w}{\partial h} = \Gamma_N \Omega_w . \quad (31)$$

For chorus emissions to grow at the equator, the temporal growth rate should be positive, namely, $\partial\Omega_w/\partial t > 0$. From (31) we therefore obtain

$$\frac{\partial\Omega_w}{\partial h} < \frac{\Gamma_N}{V_g} \Omega_w , \quad (32)$$

where we have assumed that the chorus waves propagate in the positive direction, i.e., $V_g > 0$.

We have found that chorus elements with a rising tone are generated at the equator [Katoh and Omura, 2007b; Omura et al., 2008]. The linear growth rate of the whistler mode instability maximizes at the equator because the absolute value of the resonance velocity takes the lowest value there. The flux of the resonant electrons therefore maximizes at the equator. Thus, the wave amplitude grows fastest and reaches the threshold value for the

linear wave growth at the equator. Our theory and simulations are validated by the

fact that the source location of chorus elements is indeed confirmed by recent spacecraft observations to be close to the magnetic equator [e.g., *Santolik et al.*, 2003].

At the equator the inhomogeneity of the magnetic field is zero, and the second term on the right-hand side of (10) vanishes. Since the maximum nonlinear wave growth takes place when $S = -0.4$ [Omura *et al.*, 2008], we can derive from (10) the relation between the frequency sweep rate and the normalized wave amplitude at the equator $\Omega_{w0} = eB_{w0}/m_0$ in the form,

$$\frac{\partial \omega}{\partial t} = \frac{0.4 s_0 \omega}{s_1} \Omega_{w0} \quad , \quad (33)$$

where the wave amplitude B_{w0} is compared with the static magnetic field intensity B_0 at the equator by $B_{w0}/B_0 = \Omega_{w0}/\Omega_{e0}$. Equation (2) implies that the frequency does not change in the frame of reference moving with the group velocity V_g . As we have seen in the previous section, the frequency sweep rate $\partial\omega/\partial t$ can be assumed constant for the frequency range $\omega = 0.1 \sim 0.7 \Omega_{e0}$ as the wave packet propagates along the magnetic field line.

Near the magnetic equator, we assume a parabolic variation along the magnetic field line, which is specified by the L value and the Earth's radius R_E , as expressed by $\Omega_e = \Omega_{e0}(1 + ah^2)$ with $a = 4.5/(LR_E)^2$. Noting that $\partial\Omega_e/\partial h = 2a\Omega_{e0}h$, we consider the distance h_c at which the first and second terms of the right-hand side of equation (10) become equal. Equating the two terms and using (33), we obtain the critical distance h_c as

$$h_c = \frac{s_0 \omega \Omega_{w0}}{5ca s_2 \Omega_{e0}} \quad . \quad (34)$$

distance h_c is used in identifying the dominant terms of the inhomogeneity ratio S

in the following.

As the chorus emission propagates further from the equator to the distance h ($\gg h_c$), the second term of the inhomogeneity ratio (10) becomes much greater than the first term. For the chorus element to maintain maximum growth at this distance, a negative resonant current J_E must be formed with $S = -0.4$. Neglecting the first term on the right-hand side of (10) and setting $S = -0.4$, we obtain

$$\Omega_w = \frac{cs_2}{0.4s_0\omega} \frac{\partial\Omega_e}{\partial h} . \quad (35)$$

Taking the spatial derivative of (35), we obtain

$$\frac{\partial\Omega_w}{\partial h} = \frac{cs_2}{0.4s_0\omega} \frac{\partial^2\Omega_e}{\partial h^2} = \frac{5cas_2\Omega_{e0}}{s_0\omega} . \quad (36)$$

Self-sustaining nonlinear wave growth during propagation near the equator, where the dipole magnetic field is approximated by the parabolic function, requires that the spatial gradient of the wave amplitude $\partial\Omega_w/\partial h$ is a constant as shown in (36). It should be noted that the spatial gradient of the wave amplitude does not depend on the wave amplitude itself. When the optimum self-sustaining wave growth is realized as the initial generation process of a chorus element, the gradient of the wave amplitude should be close to the value given by (36).

Inserting (36) into (32), we obtain the inequality,

$$\Omega_{w0} > \frac{5cas_2\Omega_{e0}V_g}{s_0\omega\Gamma_N} . \quad (37)$$

g the normalized parameters, $\tilde{V}_{\perp 0} = V_{\perp 0}/c$, $\tilde{\omega} = \omega/\Omega_{e0}$, $\tilde{a} = ac^2/\Omega_{e0}^2$, $\tilde{U}_{t\parallel} = U_{t\parallel}/c$,

$\tilde{\omega}_{ph} = \omega_{ph}/\Omega_{e0}$, and $\tilde{\Omega}_{w0} = \Omega_{w0}/\Omega_{e0}$, we rewrite (37) as

$$\tilde{\Omega}_{w0} = \frac{B_{w0}}{B_0} > \tilde{\Omega}_{th} \quad , \quad (38)$$

where

$$\tilde{\Omega}_{th} = \frac{100\pi^3\gamma^3\xi}{\tilde{\omega}\tilde{\omega}_{ph}^4\tilde{V}_{\perp 0}^5\delta^5} \left(\frac{\tilde{a}s_2\tilde{U}_{t\parallel}}{Q} \right)^2 \exp \left(\frac{\gamma^2\tilde{V}_R^2}{\tilde{U}_{t\parallel}^2} \right) \quad . \quad (39)$$

It is clear from (35) that the self-sustaining mechanism only works for $h > 0$ with the positive gradient of the magnetic field. That is, nonlinear wave growth takes place only when the wave propagates away from the equator with an amplitude satisfying (38). In Figure 4 we plot the amplitude threshold for typical parameters at the Earth ($L = 4.4$) and for the electron plasma frequencies $\tilde{\omega}_{pe} = 2, 3, 5, 8$. The wave amplitude threshold is higher for a lower wave frequency $\tilde{\omega}$ and for a smaller plasma frequency $\tilde{\omega}_{pe}$. Since the linear wave growth rate usually maximizes in the lower frequency range [e.g., *Omura and Summers*, 2004], the amplitude threshold becomes especially important for smaller plasma frequencies.

5. Rising tone emission

In the formulation of the mechanism of nonlinear wave growth described above we have not assumed any specific value for the temperature anisotropy. Since the resonant current induced by an electromagnetic electron hole is proportional to the average perpendicular velocity $V_{\perp 0}$, higher values of $V_{\perp 0}$ imply a higher nonlinear growth rate (see equation (22)). An additional important parameter that controls the nonlinear growth rate is the wave amplitude Ω_w . If the wave amplitude is sufficiently large to cause the nonlinear trapping of resonant electrons, then nonlinear wave growth takes place even for low values of $V_{\perp 0}$.

Therefore, nonlinear wave growth is not related to linear wave growth. Nonlinear and

linear wave growth do not coexist because the gradient of the unperturbed distribution function as assumed in the linear theory is entirely modified by the formation of the electron hole. If a wave of sufficiently large amplitude is injected into a linearly stable plasma state in the inner magnetosphere where high energy electrons are trapped, then the wave can trigger a self-sustaining emission if the amplitude exceeds the threshold given by (39).

Nonlinear wave growth is due to the formation of a resonant current as described by the second-order resonance condition; linear wave growth is due to particle diffusion at the resonance velocity determined by the first-order resonance condition. In the linear growth phase starting from incoherent thermal noise, there arises a coherency at a frequency corresponding to the maximum linear growth rate. Once the amplitude of a coherent wave exceeds the threshold value for self-sustaining emissions, nonlinear wave growth sets in, driven by the second-order phase variation $\partial\omega/\partial t$ corresponding to the maximum value of the resonant current J_E .

We evaluate the temporal variation of the wave amplitude by assuming that the spatial derivative of the wave amplitude in (31) takes the threshold value for self-sustaining wave growth given by (36). Assuming the minimum spatial gradient of the growing wave amplitude in (36), and inserting this into (31), we derive the equation,

$$\frac{\partial \tilde{\Omega}_{w0}}{\partial \tilde{t}} = \tilde{V}_g \left[\frac{Q\tilde{\omega}_{ph}^2}{2\tilde{U}_{t\parallel}} \left(\frac{\tilde{V}_{\perp 0}\delta}{\pi\gamma} \right)^{3/2} \left(\frac{\xi\tilde{\Omega}_{w0}}{\tilde{\omega}} \right)^{1/2} \exp \left(-\frac{\gamma^2\tilde{V}_R^2}{2\tilde{U}_{t\parallel}^2} \right) - \frac{5s_2\tilde{a}}{s_0\tilde{\omega}} \right]. \quad (40)$$

We now rewrite (33) in the form,

$$\frac{\partial \tilde{\omega}}{\partial \tilde{t}} = \frac{2s_0}{5s_1} \tilde{\omega} \tilde{\Omega}_{w0} \quad . \quad (41)$$

temporal evolution of a chorus element at the equator is determined by the pair of

coupled differential equations (40) and (41) for the frequency range of $0.1 \sim 0.7 \Omega_{e0}$. In this frequency range the variation of the frequency sweep rate is not significant. At higher frequencies the mechanism of the nonlinear growth breaks down because of the substantial mitigation of the frequency sweep rate through propagation.

Recently two different types of simulations have demonstrated that energetic electrons with a temperature anisotropy can produce rising chorus emissions near the magnetic equator. Examples of these simulations are Figure. In Figure 5(a) we show an electron-hybrid simulation in which the dense cold electrons are treated as a fluid while the resonant electrons are treated as super particles [Kato and Omura, 2006, 2007b]. In Figure 5(b) we show a full-particle simulation in which the energetic and cold components of electrons are treated as particles [Hikishima et al., 2009]. In both simulations, we find the frequency sweep rates of rising chorus elements are proportional to the wave amplitudes at the equator Ω_{w0} , as predicted by (33). In these simulations, we confirm that there exists a threshold value for the wave amplitude to grow due to the nonlinear wave growth mechanism, i.e., due to the formation of an electromagnetic electron hole in the velocity phase space.

We calculate the threshold amplitude $\tilde{\Omega}_{th}$ for the parameters assumed in these simulations from (39). *Katoh and Omura* [2007b] (Simulation A) assumed that $\tilde{a} = 9.8 \times 10^{-7}$, $\tilde{V}_{\perp 0} = 0.7$, $\tilde{U}_{t\parallel} = 0.35$, $\tilde{\omega}_{pe} = 4$, and $\tilde{\omega}_{ph} = 0.11$. Taking $Q = 0.5$, we then have $\tilde{\Omega}_{th} = 2.8 \times 10^{-4}$ for $\tilde{\omega} = 0.2$. In Simulation A the wave amplitude that induces the nonlinear growth is $\tilde{\Omega}_{w0} \sim 4 \times 10^{-4}$.

393 $\tilde{U}_{t\parallel} = 0.2$, $\tilde{\omega}_{pe} = 5$, and $\tilde{\omega}_{ph} = 0.40$. Setting $Q = 0.5$, we have $\tilde{\Omega}_{th} = 4 \times 10^{-4}$ for $\tilde{\omega} = 0.2$,
394 while in the simulation the wave amplitude at the onset of the rising chorus element at
395 the equator is about $\tilde{\Omega}_{w0} = 7 \times 10^{-4}$. Therefore, we confirm that our theoretical analysis
396 of the threshold for nonlinear wave growth yields approximate values for the initial wave
397 amplitudes of the chorus emissions near the equator.

398 We solve equations (40) and (41) numerically starting from the values near the threshold
399 amplitudes at $\tilde{\omega} = 0.2$. Figure 6(a) shows the calculation for Simulation A for two
400 solutions with slightly different initial wave amplitudes. One solution starting with $\tilde{\Omega}_{w0} =$
401 2.5×10^{-4} drawn as a solid curve shows a rising chorus element, while the other starting
402 with $\tilde{\Omega}_{w0} = 2.0 \times 10^{-4}$ drawn as a dashed curve just damps out. The duration time of
403 the chorus emission is about $4000 \Omega_{e0}^{-1}$ which agrees with the duration time of the first
404 few chorus elements in Figure 6(a). The calculations for Simulation B are similar to those
405 for Simulation A and result in similar solutions, but the duration time of the emissions is
406 shorter, see Figure 6(b). One solution starting with $\tilde{\Omega}_{w0} = 8 \times 10^{-4}$ shows a rising chorus
407 element, while the other in dashed curve with $\tilde{\Omega}_{w0} = 7 \times 10^{-4}$ is a diminishing element.
408 We have assumed $Q = 0.5$ for these calculations, but this is a parameter which we cannot
409 determine exactly. We have varied the value of Q which changes the threshold as given
410 by (39), but the duration time of the chorus element does not change appreciably. The
411 duration time is about $2500 \Omega_{e0}^{-1}$, which is also in agreement with the chorus elements
412 that appear in the initial phase of Simulation B, as shown in Figure 5(b).

413 In both simulations, we find that the nonlinear wave growth gives rising tone emissions
414 starting from frequencies $0.1 \sim 0.2 \Omega_{e0}$ and reaching frequencies $0.6 \sim 0.7 \Omega_{e0}$, as shown in

Figure 6. In Simulation A, we find the emissions cover the frequency range $0.2 \sim 0.7 \Omega_{e0}$

(see Figure 6 of *Hikishima et al.* [2009]), while the linear growth rate is positive in the range $0.1 \sim 0.5 \Omega_{e0}$ (Figure 2 of *Hikishima et al.* [2009]). We emphasize that the mechanism of nonlinear wave growth of chorus emissions is different from that of linear wave growth. The limitation of nonlinear wave growth comes from the breaking down of the self-sustaining mechanism in wave propagation from the equator. Since the frequency sweep rate is the key element of nonlinear wave growth, mitigation of the frequency sweep rate through propagation causes saturation of the nonlinear growth process. Assuming $h_T = h_c$ in (30), we calculate the quantity $h_c \partial \omega / \partial t$ which controls the mitigation factor D for the frequency sweep rate. For Simulation A we find $h_c = 150 \, c \Omega_{e0}^{-1}$ and $\partial \omega / \partial t = 6.7 \times 10^{-5} \, \Omega_{e0}^2$, and hence $h_c (\partial \omega / \partial t) = 0.01 \, c \Omega_{e0}$. On the other hand, for Simulation B we find $h_c = 320 \, c \Omega_{e0}^{-1}$ for $\Omega_{w0} = 3 \times 10^{-3} \Omega_{e0}$ and $\omega = 0.35 \Omega_{e0}$. Since the maximum distance from the equator in Simulation B is only $150 \, c \Omega_{e0}^{-1}$, the simulation box is not large enough to realize nonlinear wave growth driven by the spatial inhomogeneity. The wave amplitude and frequency imply from (29) that the frequency sweep rate is $\partial \omega / \partial t = 2.4 \times 10^{-4} \, \Omega_{e0}^2$.

Starting from the low frequency $\tilde{\omega} = 0.2$, the chorus elements are formed covering a frequency range reaching beyond $0.5 \Omega_{e0}$, as was also found in the chorus simulation by *Hikishima et al.* [2009]. Most of the rising tone chorus emissions observed in the magnetosphere are, however, terminated near $0.5 \Omega_{e0}$ [e.g., *Santolik et al.*, 2004]. We propose that chorus damping near $0.5 \Omega_{e0}$ is due to another nonlinear effect which we describe in the next section.

$$E_{w||} = \frac{\omega \sin \Psi}{\delta^2 \Omega_e - \omega} E_w \quad . \quad (42)$$

mode wave is given by

$$\frac{d(\gamma v_{\parallel})}{dt} = -\frac{eE_{w\parallel}}{m_0} \sin \phi + \frac{ev_{\perp}B_w}{m_0} \sin \zeta - \frac{\gamma v_{\perp}^2}{2\Omega_e} \frac{\partial \Omega_e}{\partial h} , \quad (43)$$

where $\phi = \int (\omega - kv_{\parallel}) dt$ and $\zeta = \int (\Omega - \omega + kv_{\parallel}) dt$, and the time derivative of γ is obtained

by considering variation of electron kinetic energy K as

$$\frac{d\gamma}{dt} = \frac{1}{m_0 c^2} \frac{dK}{dt} = -\frac{eE_{w\parallel}v_{\parallel}}{m_0 c^2} \sin \phi + \frac{eE_{w\perp}v_{\perp}}{m_0 c^2} \sin \zeta . \quad (44)$$

We consider energetic particles with velocities near the wave phase velocity, i.e., $v_{\parallel} \sim \omega/k$. Denoting $\bar{v}_{\parallel} = v_{\parallel} - \omega/k$, we find that $\phi = -\int k\bar{v}_{\parallel} dt$ and $\zeta = \int (\Omega_e - k\bar{v}_{\parallel}) dt$. Since the phase of the second term on the right-hand side of (44) changes very quickly with frequencies close to Ω_e , we can neglect the contribution of this term to the variation of v_{\parallel} . Solving for the time derivative of \bar{v}_{\parallel} in (44), we obtain a pair of coupled differential equations of \bar{v}_{\parallel} and ϕ

$$\frac{d\bar{v}_{\parallel}}{dt} = -\frac{eE_{w\parallel}}{\gamma m_0} \left(1 - \frac{v_{\parallel}^2}{c^2} \right) \sin \phi - \frac{v_{\perp}^2}{2\Omega_e} \frac{\partial \Omega_e}{\partial h} \quad (45)$$

and

$$\frac{d\phi}{dt} = -k\bar{v}_{\parallel} . \quad (46)$$

Assuming that $\bar{v}_{\parallel} \sim 0$, and calculating the second-order derivative of ϕ , we obtain from

(45) and (46)

$$\frac{d^2\phi}{dt^2} = \omega_{t\parallel}^2 (\sin \phi + S_{\parallel}) , \quad (47)$$

where

$$\omega_{t\parallel}^2 = \frac{ekE_{w\parallel}\delta^2}{\gamma m_0} \quad (48)$$

$$S_{\parallel} = \frac{kv_{\perp}^2}{2\omega_{te}^2\Omega_e} \frac{\partial\Omega_e}{\partial h} . \quad (49)$$

If the condition $|S_{\parallel}| < 1$ is satisfied, the parallel electric field of the whistler-mode wave packet can trap some of the energetic electrons that satisfy $v_{\parallel} \sim V_p$. The trapping results in an increase in the kinetic energy of the trapped particles by two different mechanisms. One is the phase mixing of the trapped particles with the negative gradient ($\partial g/\partial v_{\parallel} < 0$) of the velocity distribution function $g(v_{\parallel}, \phi)$ (see Figure 7). The other is transport of the energetic electrons trapped by the potential to a higher latitude. Since the density of the energetic electrons decreases at higher latitude because of reflection at the mirror points, the electrons trapped by the parallel electric field become isolated in the phase space, thus forming the resonant current J_{\parallel} . The center of the trapping potential (V_p, ϕ_c) is given by the second-order resonance condition $d^2\phi/dt^2 = 0$. From (47), we obtain the condition $\sin\phi_c + S_{\parallel} = 0$. Since we assume that the chorus element propagates in the positive h region, i.e., moves away from the equator, we find that $S_{\parallel} > 0$ and $\sin\phi_c < 0$. Taking the average over the wave phase from $\phi = 0$ to $\phi = 2\pi$, we obtain

$$\overline{E_{w\parallel}J_{\parallel}} = -\frac{e}{2\pi} \int_0^{2\pi} E_{w\parallel} \int_{-\infty}^{\infty} v_{\parallel} g_t(v_{\parallel}, \phi) \sin\phi \, dv_{\parallel} d\phi > 0 , \quad (50)$$

where $g_t(v_{\parallel}, \phi)$ is the distribution function of resonant electrons trapped by the wave potential. Thus, trapped electrons moving with the phase velocity of the wave are accelerated while they are trapped by the longitudinal wave potential. In the dipole magnetic field, both the phase velocity and group velocity increase as the distance from the equator increases. The increase of the phase velocity corresponds to an increase in kinetic

ogy of the trapped electrons. This is a further interpretation of the process whereby

the trapped electrons are accelerated.

We consider a small box of dimension equal to one wavelength which moves with the group velocity. At the boundaries of this box the flux of electromagnetic energy is zero.

Therefore, we have

$$\frac{d\overline{W}}{dt} + \overline{\mathbf{E} \cdot \mathbf{J}} = 0 \quad , \quad (51)$$

where W denotes the total wave energy in the box. Separating the resonant current \mathbf{J} into parallel and perpendicular components J_{\parallel} and J_{\perp} , we write

$$\frac{dW}{dt} = -\overline{E_{w\parallel}J_{\parallel}} - \overline{E_{w\perp}J_{\perp}} \quad . \quad (52)$$

When the first term on the left-hand side of (52) is dominant, the wave packet loses energy and undergoes the nonlinear damping.

Since we assume quasi-parallel wave propagation, we have $E_w \sim V_p B_w$ and the parallel wave electric field is given by

$$E_{w\parallel} = \frac{\omega}{\delta^2 \Omega_e - \omega} V_p B_w \sin \Psi \quad . \quad (53)$$

Substituting (48), (49), and (53) into the trapping condition $S_{\parallel} < 1$, we thereby express the necessary condition for effective nonlinear damping as $h < h_N$ where

$$h_N = \frac{\xi \delta^3 c \Omega_w \omega}{\gamma a V_{|0}^2 (\delta^2 \Omega_e - \omega)} \sin \Psi \sim \frac{V_p \Omega_w}{\gamma a V_{|0}^2} \sin \Psi \quad . \quad (54)$$

Here, we have assumed that $\omega_{pe} \gg \Omega_{e0}$, i.e., $\delta^2 \sim 1$, and that $\omega \sim 0.5 \Omega_e$.

In order to evaluate the contributions of the first and second terms on the right-hand side of (52), we compare the limiting length h_N for nonlinear damping and the characteristic

h for nonlinear growth h_c . We obtain the results,

$$\frac{h_N}{h_c} = \frac{5V_p\Omega_w \sin \Psi}{2V_{\perp 0}\Omega_{w0}}, \quad (55)$$

where we have neglected the second term in the expression (13) for s_2 .

The nonlinear trajectories of trapped electrons span the parallel velocity range $V_p - V_{t\parallel} < v_{\parallel} < V_p + V_{t\parallel}$, where $V_{t\parallel}$ is the trapping velocity given by $V_{t\parallel} = 2\omega_{t\parallel}/k$ [Omura *et al.*, 2003]. From (48) and (53), we find

$$V_{t\parallel} = 2V_p \left[\frac{\Omega_w \delta^2 \sin \Psi}{\gamma(\delta^2 \Omega_e - \omega)} \right]^{1/2} \sim 2^{3/2} V_p \left[\frac{B_w \sin \Psi}{\gamma B_0} \right]^{1/2}, \quad (56)$$

where we have assumed that $\delta^2 \sim 1$ and $\omega \sim 0.5 \Omega_e$.

In the course of the generation of a rising tone chorus element, waves with frequencies near half the gyrofrequency can also be generated near the magnetic equator during the process of nonlinear wave growth. Before leaving the equatorial region ($h < h_N$), however, the waves lose a substantial amount of energy to the Landau resonant electrons due to the deviation of the wave number vector from the parallel direction of the geomagnetic field. Since the magnitude of the resonant current depends on the width of the trapping potential (which is itself proportional to the trapping velocity), the rate of the nonlinear damping is proportional to $\sqrt{B_w \sin \Psi}$. As waves grow with a rising frequency at the equator, wave amplitudes can be larger at higher frequencies near half the gyrofrequency. However, the larger amplitude waves with frequencies close to half the gyrofrequency are subject to stronger nonlinear damping as they propagate along the magnetic field line.

7. Comparison with observations

Rising tone emissions are observed to be split into two different frequency bands divided by the electron half-gyrofrequency, as shown in Figure 8. They are usually referred to

wer-band and upper-band chorus emissions. As we have found in the previous sec-

tion, there occurs a nonlinear longitudinal damping of the wave because the longitudinal electric field resulting from oblique propagation can interact with energetic electrons very effectively at half the gyrofrequency. Since parallel propagation is assumed in Simulations A and B, we cannot find the damping of the emissions at half the gyrofrequency.

Figure 8(a) shows observations of chorus in the Earth’s magnetosphere observed by the Cluster spacecraft [Santolik *et al.*, 2003; Santolik, 2008]. The physical parameters for this observation are the followings: $f_{c0} = 8000$ Hz, $\tilde{\omega}_{pe} = 2.4$, $R_E = 6380$ km, $L = 4.4$, $\tilde{a} = 2.0 \times 10^{-7}$. Where f_{c0} is the electron gyrofrequency at the equator in Hz, which is converted to the static magnetic field intensity B_0 in nT by $f_{c0} = 28B_0$. Assuming the parameters for energetic electrons as $T_{\perp}/T_{\parallel} = 1.5$, 20 keV, $\tilde{V}_{\perp 0} = 0.21$, $\tilde{U}_{\parallel} = 0.18$, $N_h = 0.05 N_{e0}$, we calculate the threshold for nonlinear wave growth at the equator. The threshold $\tilde{\Omega}_{th}$ changes sharply from 1×10^{-3} ($\tilde{\omega} = 0.25$) to 2×10^{-8} ($\tilde{\omega} = 0.6$). The lower plasma frequency makes the frequency range of chorus emissions to the higher frequency, enhancing the upper-band chorus.

With these parameters we also solve the chorus equations (40) and (41) with a value close to the threshold, i.e., $\tilde{\Omega}_{w0} = 1 \times 10^{-3}$ at $\tilde{\omega} = 0.26$. The result is shown in Figure 9(a). We assume that the generation of the chorus element occurs at the equator, and that the chorus element is free from longitudinal damping at the point of wave growth. As the wave packet of the rising chorus element propagates away from the equator, the part of the element at half the gyrofrequency undergoes longitudinal damping, making the chorus elements split into two parts, namely into lower-band and upper-band emissions. The duration time scale for the chorus element to undergo the nonlinear wave growth at

quator is about 100 ms, which agrees with the observations of chorus elements shown

in Figure 8(a).

Figure 8(b) shows observations of chorus at Saturn [*Hospodarsky et al.*, 2008]. Using the parameters of the associated observations of energetic electrons at Saturn [*Menietti et al.*, 2008], we calculate the threshold amplitude for the nonlinear growth of chorus elements at Saturn. The physical parameters are the followings: $f_{c0} = 1300$ Hz, $\tilde{\omega}_{pe} = 15$, $R_s = 60,000$ km, $L = 7.0$, $\tilde{a} = 3.4 \times 10^{-8}$, $T_{\perp}/T_{\parallel} = 1.5$, 20 keV, $\tilde{V}_{\perp 0} = 0.21$, $\tilde{U}_{\parallel} = 0.18$, and $N_h = 0.0001 N_{e0}$. Because of the high electron plasma frequency and the low gradient of the magnetic field, the threshold becomes as low as $\tilde{\Omega}_{th} = 3 \times 10^{-8}$. Therefore, the amplitude threshold is well satisfied by a low wave amplitude at which a whistler-mode instability with a small linear growth rate may saturate.

We also solve the chorus equations with the initial amplitude $\tilde{\Omega}_{w0} = 2.5 \times 10^{-6}$ and the initial frequency $\tilde{\omega} = 0.3$. As shown in Figure 9(b), the solution shows a rising chorus element with a duration time of 5 s. The very long duration time agrees with the duration time of chorus elements observed at Saturn [*Hospodarsky et al.*, 2008].

8. Summary and Discussion

We have further investigated the nonlinear growth mechanism of chorus emissions originally proposed by *Omura et al.* [2008], and we obtain a theoretical expression for the nonlinear growth rate Γ_N (given by (22)). From the condition of absolute instability, in which the wave grows at a localized region near the magnetic equator, we have derived the wave amplitude threshold (given by (38) and (39)) for nonlinear growth to take place in the inhomogeneous magnetic field. When the threshold condition is satisfied at the equator a rising emission is generated to form a seed of a chorus element that spans over

frequency range 0.1 - 0.7 Ω_{e0} . The upper limit comes from the dispersion effect that

invalidates the assumption of the nonlinear growth due to the large frequency sweep rate.

As the seed of chorus element propagates away from the equator in a self-sustaining man-

ner, the much slower group and phase velocities at higher frequency range ($\omega > 0.7 \Omega_{e0}$)

reduce the frequency sweep rate to a much smaller value. Since the large frequency sweep

rate is a necessary condition for the nonlinear wave growth near the equator, the reduction

of the frequency sweep rate at higher frequencies causes termination of the nonlinear wave

growth. The part of the chorus element at half the gyrofrequency is subject to longitu-

dinal wave damping arising from slightly oblique propagation. The emission is split into

lower and upper bands at half the gyrofrequency.

The gap in the wave spectrum at half the gyrofrequency has been discussed in previous

studies in terms of Landau damping under the assumption of oblique propagation [*Tsuru-*

tani and Smith, 1974; Coroniti et al., 1984]. However, the nonlinear longitudinal damping

described in section 6 is different from “classical” Landau damping which depends on the

gradient of the velocity distribution function. The nonlinear damping is due to the inho-

mogeneity of the static magnetic field rather than the gradient of the distribution function

at the phase velocity. This is very similar to the concept of nonlinear wave growth due to

the electron hole, in which the finite inhomogeneity ratio S in (10) plays an essential role.

We have derived a pair of coupled equations (40) and (41) describing the variation

of the wave amplitude and wave frequency. We call these as “chorus equations” because

their solutions agree very well with the amplitude thresholds and duration times of chorus

elements reproduced by our simulations. The chorus equations also give reasonable seed

wave solutions for the observed chorus emissions in the magnetospheres of both Earth and

rn. The difference in the duration time of chorus elements is due to the difference in

the plasma frequency $\tilde{\omega}_{pe}$ which contribute to ξ in the first term in brackets on the left-hand side of (40) and the inhomogeneity \tilde{a} in the background magnetic field in the second term in the brackets. The solutions of the chorus equations show explosive variations in the wave amplitude and the frequency, though these are not typically observed in reality or in the simulations. It may be the case that the electron hole factor Q could suppress the explosive wave growth. The rapid variation of the resonance velocity may cause an efficient entrapping of electrons that subsequently fill the electron hole thereby making Q much smaller. Further simulation studies are needed to evaluate Q .

Triggered emissions, as observed in the Siple experiment [Helliwell, 1988] and the HAARP experiment [Golkowski *et al.*, 2008], can be explained in terms of nonlinear wave growth induced by finite amplitude whistler-mode waves injected into the magnetosphere. Nonlinear wave growth is due to the formation of an electromagnetic electron hole, and differs greatly from linear growth. Even if a plasma medium with energetic electrons is linearly stable, nonlinear growth will occur in the presence of a finite amplitude wave and a sufficient flux of energetic electrons. The chorus equations (40) and (41) and the concept of wave amplitude threshold introduced in this paper should also be applicable to triggered emissions.

The nonlinear growth theory has been developed for chorus emissions with rising tones. Falling tone emissions have also been observed in the magnetosphere, although they are not so common [Matsumoto *et al.*, 1998; Santolik *et al.*, 2003]. In order to be applicable to falling tone emissions, the analysis presented herein requires subtle modifications. We leave this as a target of future theory and simulations.

acknowledgments. This work was partially supported by Grant-in-Aid 20340135 and

17GS0208 for Creative Scientific Research “The Basic Study of Space Weather Prediction”
of the Ministry of Education, Science, Sports and Culture of Japan, and International
Communication Foundation. D. S. acknowledges support from the Natural Sciences and
Engineering Research Council of Canada under grant A-0621 and additional support by
WCU grant (No. R31-10016) funded by the Korean Ministry of Education, Science and
Technology.

References

- Albert, J. M. (2000), Gyroresonant interactions of radiation belt particles with a
monochromatic electromagnetic wave, *J. Geophys. Res.*, *105*, A9, 21,191.
- Albert, J. M. (2002), Nonlinear interaction of outer zone electrons with VLF waves,
Geophys. Res. Lett., *29*(8), 1275, doi:10.1029/2001GL01394.
- Anderson, R. R., and W. S. Kurth (1989), Discrete electromagnetic emissions in planetary
magnetospheres, In *Plasma Waves and Instabilities at Comets and in Magnetospheres*,
Geophys. Monogr. Ser., *53*, edited by B. T. Tsurutani and H. Oya, p. 81, AGU, Wash-
ington, D.C..
- Bortnik, J., U. S. Inan, and T. F. Bell (2006), Landau damping and resul-
tant unidirectional propagation of chorus waves, *Geophys. Res. Lett.*, *33*, L03102,
doi:10.1029/2005GL024553.
- Coroniti F. V., F. L. Scarf, and C. F. Kennel (1984), Analysis of Chorus Emissions at
Jupiter, *J. Geophys. Res.*, *89*, 3801.

ya, N., Y. Omura, and D. Summers (2008), Relativistic turning acceleration of

radiation belt electrons by whistler mode chorus, *J. Geophys. Res.*, *113*, A04224,
doi:10.1029/2007JA012478.

Golkowski, M., U. S. Inan, A. R. Gibby, and M. B. Cohen (2008), Magnetospheric ampli-
fication and emission triggering by ELF/VLF waves injected by the 3.6 MW HAARP
ionospheric heater, *J. Geophys. Res.*, *113*, A10201, doi:10.1029/2008JA013157.

Helliwell, R. A. (1988), VLF wave simulation experiments in the magnetosphere from
Siple Station, *Antarctica, Rev. Geophys.*, *26*, 551. 578.

Hikishima, M., S. Yagitani, Y. Omura, and I. Nagano (2009), Full particle simulation
of whistler-mode rising chorus emissions in the magnetosphere, *J. Geophys. Res.*, *114*,
A01203, doi:10.1029/2008JA013625.

Horne, R. B., R. M. Thorne, S. A. Glauert, J. M. Albert, N. P. Meredith, and R. R.
Anderson (2005), Timescale for radiation belt electron acceleration by whistler mode
chorus waves, *J. Geophys. Res.*, *110*, A03225, doi: 10.1029/2004JA00811.

Hospodarsky, G. B., T. F. Averkamp, W. S. Kurth, D. A. Gurnett, J. D. Menietti, O.
Santolik, and M. K. Dougherty (2008), Observations of chorus at Saturn using the
Cassini Radio and Plasma Wave Science instrument, *J. Geophys. Res.*, *113*, A12206,
doi:10.1029/2008JA013237.

Inan, U. S., T. F. Bell, J. Bortnik, and J. M. Albert (2003), Controlled precipitation of
radiation belt electrons, *J. Geophys. Res.*, *108*(A5), 1186, doi:10.1029/2002JA009580.

Inan, U. S., M. Platino, and T. F. Bell, D. A. Gurnett, and J. S. Pickett (2004), Cluster
measurements of rapidly moving sources of ELV/VLF chorus, *J. Geophys. Res.*, *109*,
A05214, doi: 10.1029/2003JA010289.

B. T. Tsurutani (2009), Simultaneous satellite observations of VLF chorus, hot and relativistic electrons in a magnetic storm “ recovery ” phase, *Geophys. Res. Lett.*, *36*, L01106, doi:10.1029/2008GL036454.

Katoh, Y. and Y. Omura (2004), Acceleration of relativistic electrons due to resonant scattering by whistler mode waves generated by temperature anisotropy in the inner magnetosphere, *J. Geophys. Res.*, *109*, A12214, doi: 10.1029/2004JA010654.

Katoh, Y. and Y. Omura (2006), A study of generation mechanism of VLF triggered emission by self-consistent particle code, *J. Geophys. Res.*, *111*, A12207, doi:10.1029/2006JA011704.

Katoh, Y. and Y. Omura (2007a), Relativistic particle acceleration in the process of whistler-mode chorus wave generation, *Geophys. Res. Lett.*, *34*, L13102, doi:10.1029/2007GL029758.

Katoh, Y. and Y. Omura (2007b), Computer simulation of chorus wave generation in the Earth’s inner magnetosphere, *Geophys. Res. Lett.*, *34*, L03102, doi:10.1029/2006GL028594.

Katoh, Y., Y. Omura, and D. Summers (2008), Rapid energization of radiation belt electrons by nonlinear wave trapping, *Ann. Geophys.*, *26*, 3451.

Lauben, D. S., U. S. Inan, T. F. Bell, D. L. Kirchner, S. B. Hospodarsky, and J. S. Pickett (1998), VLF chorus emissions observed by Polar during the January 10, 1997 magnetic cloud, *Geophys. Res. Lett.*, *25*, 2995.

Lauben, D. S., U. S. Inan, T. F. Bell, and D. A. Gurnett (2002), Source characteristics of ELF/VLF chorus, *J. Geophys. Res.*, *107*, 1429, doi:10.1029/2000JA003019.

sumoto, H., and Y. Omura (1981), **Cluster and channel effect phase bunching by**

whistler waves in the nonuniform geomagnetic field, *J. Geophys. Res.*, **86**, 779.

Matsumoto, H., H. Kojima, Y. Omura, and I. Nagano (1998), Plasma Waves in Geospace:

GEOTAIL Observations, *New Perspectives on the Earth's Magnetotail*, *Geophysical Monograph Series*, American Geophysical Union, 105, 259.

Menietti, J. D., O. Santolik, A. M. Rymer, G. B. Hospodarsky, A. M. Persoon, D. A.

Gurnett, A. J Coates, and D. T. Young (2008), Analysis of plasma waves observed within local plasma injections seen in Saturn's magnetosphere, *J. Geophys. Res.*, *113*, A05213, doi:10.1029/2007JA012856.

Miyoshi, Y., A. Morioka, T. Obara, H. Misawa, T. Nagai, and Y. Kasahara (2003), Rebuilding process of the outer radiation belt during the 3 November 1993 magnetic storm: NOAA and Exos-D observations, *J. Geophys. Res.*, *108* (A1), 1004, doi: 10.1029/2001JA007542.

Nunn, D. (1974), A self-consistent theory of triggered VLF emissions, *Planet. Space Sci.*, **22**, 349.

Nunn, D., Y. Omura, H. Matsumoto, I. Nagano, and S. Yagitani (1997), The numerical simulation of VLF chorus and discrete emissions observed on the Geotail satellite using a Vlasov code, *J. Geophys. Res.*, *102*, 27083.

Omura, Y., and H. Matsumoto (1982), Computer simulations of basic processes of coherent whistler wave-particle interactions in the magnetosphere, *J. Geophys. Res.*, 87, 4435.

Omura, Y., and D. Summers (2004), Computer simulations of relativistic whistler-mode wave-particle interactions, *Phys. Plasmas*, *11*, 3530.

Ira, Y., and D. Summers (2006), Dynamics of high-energy electrons interacting with

whistler mode chorus emissions in the magnetosphere, *J. Geophys. Res.*, *111*, A09222,
doi:10.1029/2006JA011600.

Omura, Y., D. Nunn, H. Matsumoto, and M. J. Rycroft (1991), A review of observational,
theoretical and numerical studies of VLF triggered emissions, *J. Atmos. Terr. Phys.*,
53, 351.

Omura, Y., T. Umeda, and H. Matsumoto (2003), Simulation of Electron Beam Insta-
bilities and Nonlinear Potential Structures, *Space Plasma Simulation, edited by Joerg*
Buechner et al., Springer- Berlag Berlin Heidelberg, pages 79-92.

Omura, Y., N. Furuya, and D. Summers (2007), Relativistic turning acceleration of reso-
nant electrons by coherent whistler mode waves in a dipole magnetic field, *J. Geophys.*
Res., *112*, A06236, doi:10.1029/2006JA012243.

Omura, Y., Y. Katoh, and D. Summers (2008), Theory and simulation of the generation
of whistler-mode chorus, *J. Geophys. Res.*, *113*, A04223, doi:10.1029/2007JA012622.

Roth, I., M. Temerin, and M. K. Hudson (1999), Resonant enhancement of relativistic
electron fluxes during geomagnetically active periods, *Ann. Geophys.*, *17*, 631.

Santolik, O., D. A. Gurnett, and J. S. Pickett, Multipoint investigation of the source
region of storm-time chorus (2004), *Ann. Geophys.*, *22*, 2255.

Santolik, O., D. A. Gurnett, J. S. Pickett, M. Parrot, and N. Cornilleau-Wehrlin (2003),
Spatio-temporal structure of storm-time chorus, *J. Geophys. Res.*, *108* (A7), 1278,
doi:10.1029/2002JA00979

Santolik, O., D. A. Gurnett, J. S. Pickett, M Parrot, and N. Cornilleau-Wehrlin (2004),
A microscopic and nanoscopic view of storm-time chorus on 31 March 2001, *Geophys.*

756 Santolik, O. (2008), New results of investigations of whistler-mode chorus emissions, *Non-*
757 *lin. Processes Geophys.*, *15*, 621.

758 Stix, T. H. (1992), *Waves in Plasmas*, American Institute of Physics, New York.

759 Summers, D., and Y. Omura (2007), Ultra-relativistic acceleration of electrons in plane-
760 tary magnetospheres, *Geophys. Res. Lett.*, *34*, L24205, doi:10.1029/2007GL032226.

761 Summers, D., and C. Ma (2000), A model for generating relativistic electrons in the
762 Earth's inner magnetosphere based on gyroresonant wave-particle interactions, *J. Geo-*
763 *phys. Res.*, *105*, 2625.

764 Summers, D., R. M. Thorne, and F. Xiao (1998), Relativistic theory of wave-particle
765 resonant diffusion with application to electron acceleration in the magnetosphere, *J.*
766 *Geophys. Res.*, *103*, 20487.

767 Summers, D., C. Ma, N. P. Meredith, R. B. Horne, R. M. Thorne, D. Heynderickx, and
768 R. R. Anderson (2002), Model of the energization of outer-zone electrons by whistler-
769 mode chorus during the October 9, 1990 geomagnetic storm, *Geophys. Res. Lett.*, *29*
770 (4), 2174, doi: 10.1029/2002GL016039.

771 Summers, D., C. Ma, N. P. Meredith, R. B. Horne, R. M. Thorne, and R. R. Ander-
772 son (2004a), Modeling outer-zone relativistic electron response to whistler-mode chorus
773 activity during substorms, *J. Atmos. Solar-Terr. Phys.*, *66*, 133.

774 Summers, D., C. Ma, and T. Mukai (2004b), Competition between acceleration and loss
775 mechanisms of relativistic electrons during geomagnetic storms, *J. Geophys. Res.*, *109*,
776 A04221, doi:10.1029/2004JA010437.

mers, D., B. Ni, and N. P. Meredith (2007a), Timescales for radiation belt electron

acceleration and loss due to resonant wave-particle interactions: 1. Theory, *J. Geophys. Res.*, *112*, A04206, doi:10.1029/2006JA011801.

Summers, D., B. Ni, and N. P. Meredith (2007b), Timescales for radiation belt electron acceleration and loss due to resonant wave-particle interactions: 2. Evaluation for VLF chorus, ELF hiss, and EMIC waves, *J. Geophys. Res.*, *112*, A04207, doi:10.1029/2006JA011993.

Trakhtengerts, V. Y. (1995), Magnetosphere cyclotron maser: Backward wave oscillator generation regime, *J. Geophys. Res.*, *100*, 17205.

Trakhtengerts, V. Y. (1999), A generation mechanism for chorus emission, *Anal. Geophysicae*, *17*, 95.

Tsurutani, B. T., and E. J. Smith (1974), Postmidnight chorus: A substorm phenomenon, *J. Geophys. Res.*, *79*, 118.

We rewrite the cold plasma dispersion relation (3) as

$$c^2 k^2 = \omega^2 + \frac{\omega \omega_{pe}^2}{\Omega_e - \omega} \quad (\text{A1})$$

with $\omega_{pe}^2 = N_e e^2 / (\epsilon_0 m_0)$, where N_e is the cold electron density. Assuming $N_e(h)/N_{e0} = \Omega_e(h)/\Omega_{e0}$, we obtain

$$\frac{\partial(\omega_{pe}^2)}{\partial h} = \frac{\omega_{pe}^2}{\Omega_e} \frac{\partial \Omega_e}{\partial h} \quad , \quad (\text{A2})$$

Differentiating both sides of (A1) with respect to h , and solving for $\partial k / \partial h$, we obtain

$$\frac{\partial k}{\partial h} = -V_g^{-1} \frac{\partial k}{\partial t} - \frac{\omega^2 \delta}{2c\xi \Omega_e (\Omega_e - \omega)} \frac{\partial \Omega_e}{\partial h} \quad . \quad (\text{A3})$$

We also differentiate equation (A1) with respect to time t to obtain

$$\frac{\partial \omega}{\partial t} = -V_g \frac{\partial \omega}{\partial h} \quad . \quad (\text{A4})$$

From the cyclotron resonance condition,

$$V_R = \frac{\omega - \Omega_e / \gamma}{k} \quad , \quad (\text{A5})$$

we calculate dV_R/dt as seen by a particle moving with a parallel velocity v_{\parallel} . Following the same procedure as described in *Omura et al.* [2008], we obtain

$$\frac{dV_R}{dt} = \frac{\Omega_e}{k\gamma^2} \frac{d\gamma}{dt} + \frac{1}{k} \left(1 - \frac{V_R}{V_g}\right) \left(1 - \frac{v_{\parallel}}{V_g}\right) \frac{\partial \omega}{\partial t} - \frac{v_{\parallel}}{\gamma k} \left\{1 + \frac{\omega \delta^2 (\Omega_e - \gamma \omega)}{2\Omega_e (\Omega_e - \omega)}\right\} \frac{\partial \Omega_e}{\partial h} \quad . \quad (\text{A6})$$

The electron equation of motion is

$$\frac{dv_{\parallel}}{dt} = \frac{\Omega_w v_{\perp}}{\gamma} \sin \zeta - \frac{v_{\parallel}}{\gamma} \frac{d\gamma}{dt} - \frac{v_{\perp}^2}{2\Omega_e} \frac{\partial \Omega_e}{\partial h} \quad . \quad (\text{A7})$$

Considering the variation of the electron kinetic energy, we write

$$\frac{d\gamma}{dt} = \frac{\Omega_w \omega v_{\perp}}{kc^2} \sin \zeta \quad . \quad (\text{A8})$$

first-order resonance condition $v_{\parallel} = V_R$ implies that $d\zeta/dt = k(v_{\parallel} - V_R) = 0$. To ob-

tain second-order resonance condition $d^2\zeta/dt^2 = 0$, we calculate the second-order deriva-

tive of the phase ζ ,

$$\frac{d^2\zeta}{dt^2} = k \left[\frac{d(v_{\parallel} - V_R)}{dt} \right] = k \left(\frac{dv_{\parallel}}{dt} - \frac{dV_R}{dt} \right) , \quad (\text{A9})$$

where we assumed $(v_{\parallel} - V_R) \sim 0$. Inserting (A6), (A7), and (A8) into (A9), we derive the

result,

$$\frac{d^2\zeta}{dt^2} = \frac{\omega_e^2 \delta^2}{\gamma} (\sin\zeta + S) , \quad (\text{A10})$$

where

$$S = -\frac{1}{\omega_e^2 \delta^2} \left\{ \gamma \left(1 - \frac{V_R}{V_g} \right)^2 \frac{\partial \omega}{\partial t} + \left[\frac{k\gamma v_{\perp}^2}{2\Omega_e} - \left(1 + \frac{\omega}{\Omega_e} \frac{\delta^2}{2} \frac{\Omega_e - \gamma\omega}{\Omega_e - \omega} \right) V_R \right] \frac{\partial \Omega_e}{\partial h} \right\} . \quad (\text{A11})$$

The equation $d^2\zeta/dt^2 = 0$ gives the second-order cyclotron resonance condition for elec-
trons stably trapped by the wave.

Appendix B: Derivative of the group velocity

We differentiate the group velocity V_g with respect to ω , noting that derivatives of ξ
and δ are given by

$$\frac{\partial \xi}{\partial \omega} = \frac{\Omega_e - 2\omega}{2\omega_{pe}^2 \xi} \quad (\text{B1})$$

and

$$\frac{\partial \delta}{\partial \omega} = \frac{\partial \delta}{\partial \xi} \frac{\partial \xi}{\partial \omega} = -\frac{\delta^3 (\Omega_e - 2\omega)}{2\omega_{pe}^2} . \quad (\text{B2})$$

We obtain from (7)

$$\frac{\partial V_g}{\partial \omega} = \frac{V_g}{\xi} \left\{ \frac{\partial \xi}{\partial \omega} - \frac{\xi}{\delta} \frac{\partial \delta}{\partial \omega} - \frac{V_g \delta}{c} \left[2\xi \frac{\partial \xi}{\partial \omega} + \frac{\Omega_e}{2(\Omega_e - \omega)^2} \right] \right\} . \quad (\text{B3})$$

stituting (B1) and (B2) into (B3) and using (3), we find

$$\frac{\partial V_g}{\partial \omega} = \frac{\xi^2 V_g (\Omega_e - 2\omega)}{2\omega (\Omega_e - \omega)} \left\{ \frac{1}{\xi^2} + \frac{1}{1 + \xi^2} - \frac{V_g \delta}{c\xi} \left[2 + \frac{\Omega_e \omega}{\xi^2 (\Omega_e - 2\omega) (\Omega_e - \omega)} \right] \right\}. \quad (\text{B4})$$

Making use of (3) and (7), we obtain

$$\frac{\partial V_g}{\partial \omega} = \frac{V_g^2 \delta^3}{4c\xi\omega(\Omega_e - \omega)^2} (\Omega_e^2 - 4\omega\Omega_e - 4\xi^2\omega^2) \quad . \quad (\text{B5})$$

Using (3), we factorize the quadratic in Ω_e in (B5) to obtain (27).

Appendix C: Polarization of a whistler-mode wave for quasi-parallel propagation

The static magnetic field \mathbf{B}_o is taken in the z direction, We assume a wave electric field (E_x, E_y, E_z) with a frequency ω , and with a wave number vector $\mathbf{k} = (k \cos \Psi, 0, k \sin \Psi)$ where Ψ is the wavenormal angle. From *Stix* [1992], the wave electric field (E_x, E_y, E_z) for a homogeneous plasma satisfies

$$\begin{bmatrix} S - n^2 \cos^2 \Psi & -iD & n^2 \cos \Psi \sin \Psi \\ iD & S - n^2 & 0 \\ n^2 \cos \Psi \sin \Psi & 0 & P - n^2 \sin^2 \Psi \end{bmatrix} \begin{bmatrix} E_x \\ E_y \\ E_z \end{bmatrix} = 0 \quad (\text{C1})$$

where

$$n = \frac{ck}{\omega} \quad , \quad (\text{C2})$$

and P , S , and D are given by

$$P = 1 - \frac{\Omega_e - \omega}{\omega \xi^2} \quad , \quad (\text{C3})$$

$$S = 1 + \frac{\omega}{(\Omega_e + \omega)\xi^2} \quad , \quad (\text{C4})$$

and

$$D = \frac{\Omega_e}{(\Omega_e + \omega)\xi^2} \quad . \quad (\text{C5})$$

if a non-zero electric field, the determinant of the matrix is zero. Namely, we obtain

$$(P - n^2 \sin^2 \Psi) \{ (S - n^2)(S - n^2 \cos^2 \Psi) - D^2 \} - n^4 (S - n^2) \cos^2 \Psi \sin^2 \Psi = 0 \quad , \quad (\text{C6})$$

We assume quasi-parallel wave propagation in which $\sin^2 \Psi \ll 1$, while we retain the term in $\sin \Psi$. We then find

$$P(S - n^2 - D)(S - n^2 + D) = 0 \quad . \quad (\text{C7})$$

For the transverse whistler-mode waves, we have

$$n^2 = S + D \quad , \quad (\text{C8})$$

which we rewrite as

$$\delta^2 = \frac{1}{1 + \xi^2} \quad . \quad (\text{C9})$$

This result is identical to the cold plasma dispersion relation for purely parallel propagation.

The polarization relations are given by

$$E_z = \frac{n^2 \cos \Psi \sin \Psi}{n^2 \sin^2 \Psi - P} E_x \quad (\text{C10})$$

and

$$E_y = \frac{iD}{n^2 - S} E_x \quad . \quad (\text{C11})$$

Assuming quasi-parallel propagation and substituting (C3) and (C2) into (C10) and (C11), we obtain

$$E_z = \frac{\omega \sin \Psi}{\delta^2 \Omega_e - \omega} E_x \quad (\text{C12})$$

and

$$E_y = iE_x \quad . \quad (\text{C13})$$

While the E_z component appears parallel to the static magnetic field, the polarization of

894 the wave field in the plane perpendicular to the static magnetic field remains circular.

Figure 1. Nonlinear growth rate Γ_N as a function of wave frequency ω for the plasma frequencies $\omega_{pe}/\Omega_{e0} = 2, 4, 8, 16$ and the parameters $U_{t\parallel}/c = 0.18$, $V_{\perp 0}/c = 0.21$, $\omega_{ph}/\Omega_{e0} = 0.2$, $Q = 0.5$, and $\Omega_w/\Omega_{e0} = 0.0001$.

Figure 2. Schematic illustration for the variation of the frequency sweep rate.

Figure 3. (a) The group velocity V_g and the phase velocity V_p as functions of frequency ω . (b) The frequency sweep rate factor for different values of $h_T(\partial\omega/\partial t)_{h=0}$ with $\omega_{pe}/\Omega_{e0} = 4$.

Figure 4. The wave amplitude threshold for the generation of self-sustaining chorus emissions for the plasma frequencies $\tilde{\omega}_{pe} = 2, 3, 5, 8$, (indicated by the attached numbers) and for the parameters $\tilde{U}_{t\parallel} = 0.18$, $\tilde{V}_{\perp 0} = 0.21$, $\tilde{a} = 2 \times 10^{-7}$, $\tilde{\omega}_{ph} = 0.2$, and $Q = 0.5$.

Figure 5. Dynamic spectra of the chorus elements reproduced by (a) Simulation A: the electron-hybrid code [*after Omura et al.*, 2008], and by (b) Simulation B: by the full-particle code [*after Hikishima et al.*, 2009].

Figure 6. Solutions of the chorus equations for parameters used in (a) Simulation A and (b) Simulation B. The dashed line shows a solution below the amplitude threshold in each case.

Figure 7. Schematic illustration of the distribution function of energetic electrons interacting with the longitudinal component of the whistler-mode wave packet propagating away from the magnetic equator.

Figure 8. (a) Chorus emissions observed by the Cluster spacecraft in the Earth's magnetosphere ($L = 4.4$) [*after Santolik et al.*, 2003]. (b) Chorus emissions observed by the Cassini spacecraft in Saturn's magnetosphere ($L = 7.0$) [*after Hospodarsky et al.*, 2008].

Figure 9. Solutions of the chorus equations (40) and (41) using parameters for (a) the Earth ($L = 4.4$) and (b) Saturn ($L = 7.0$).

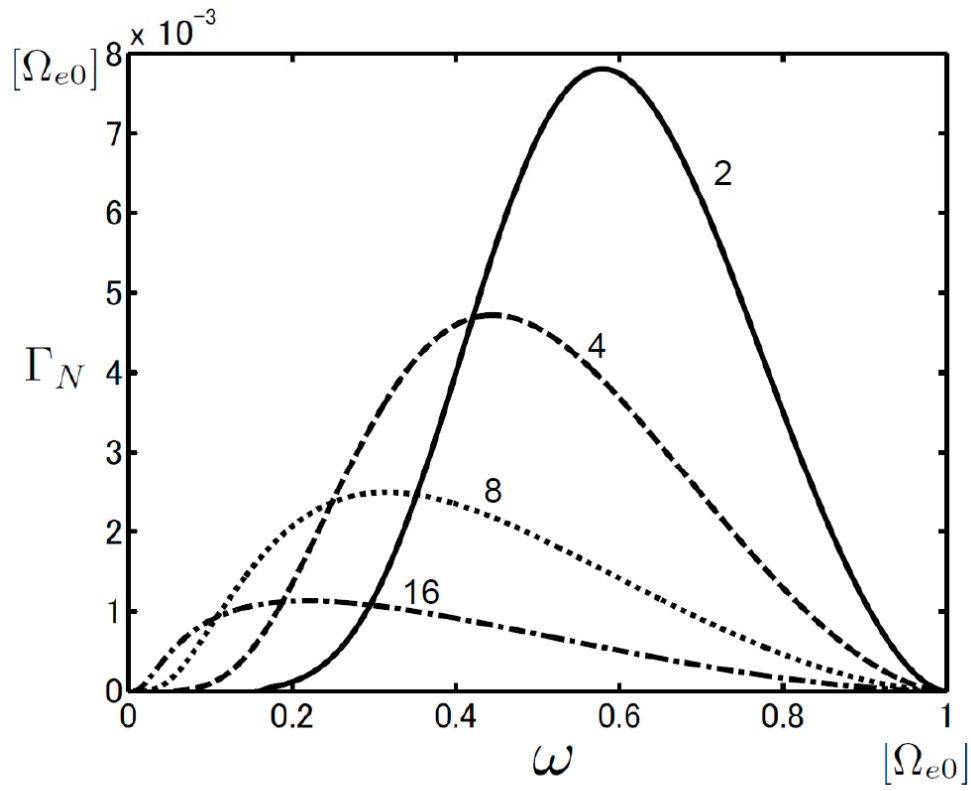


Figure 1. Nonlinear growth rate Γ_N as a function of wave frequency ω for the plasma frequencies $\omega_{pe}/\Omega_{e0} = 2, 4, 8, 16$ and the parameters $U_{t\parallel}/c = 0.18$, $V_{\perp 0}/c = 0.21$, $\omega_{ph}/\Omega_{e0} = 0.2$, $Q = 0.5$, and $\Omega_w/\Omega_{e0} = 0.0001$.

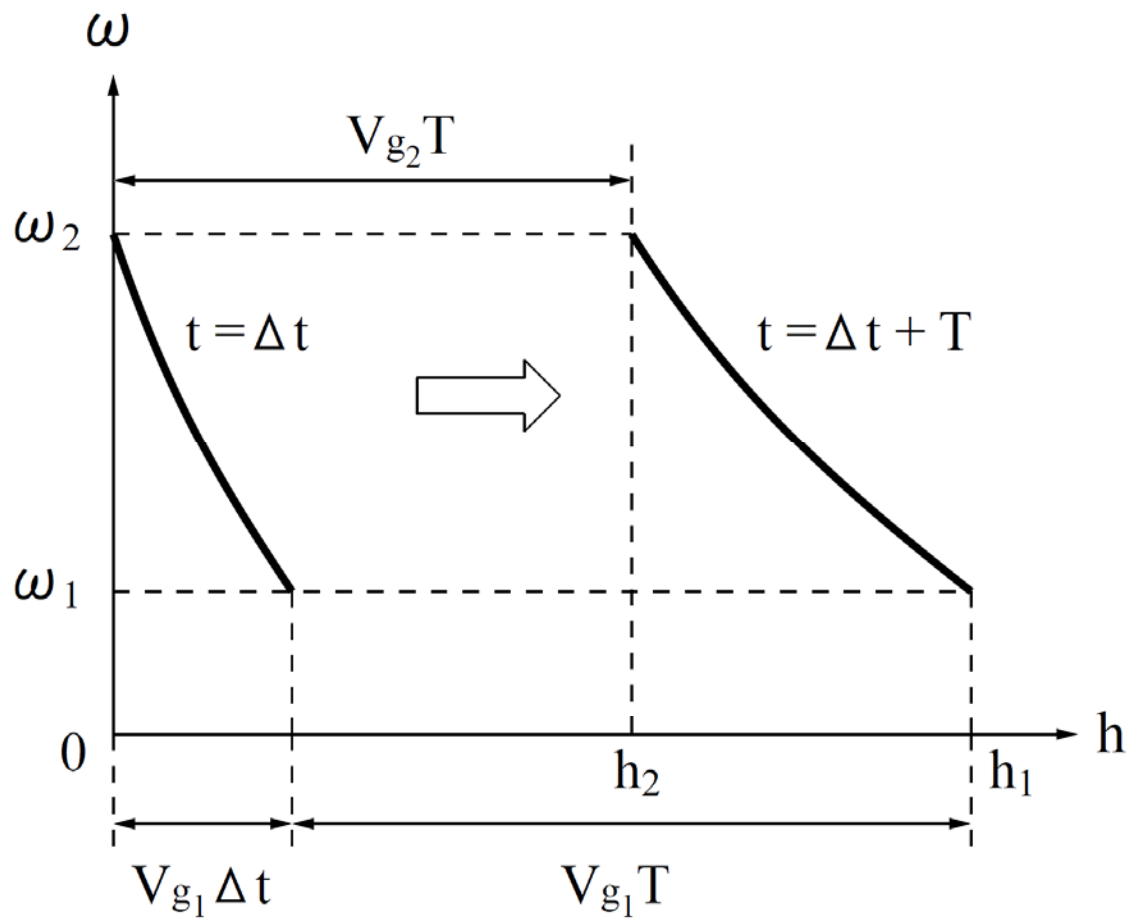


Figure 2. Schematic illustration for the variation of the frequency sweep rate.

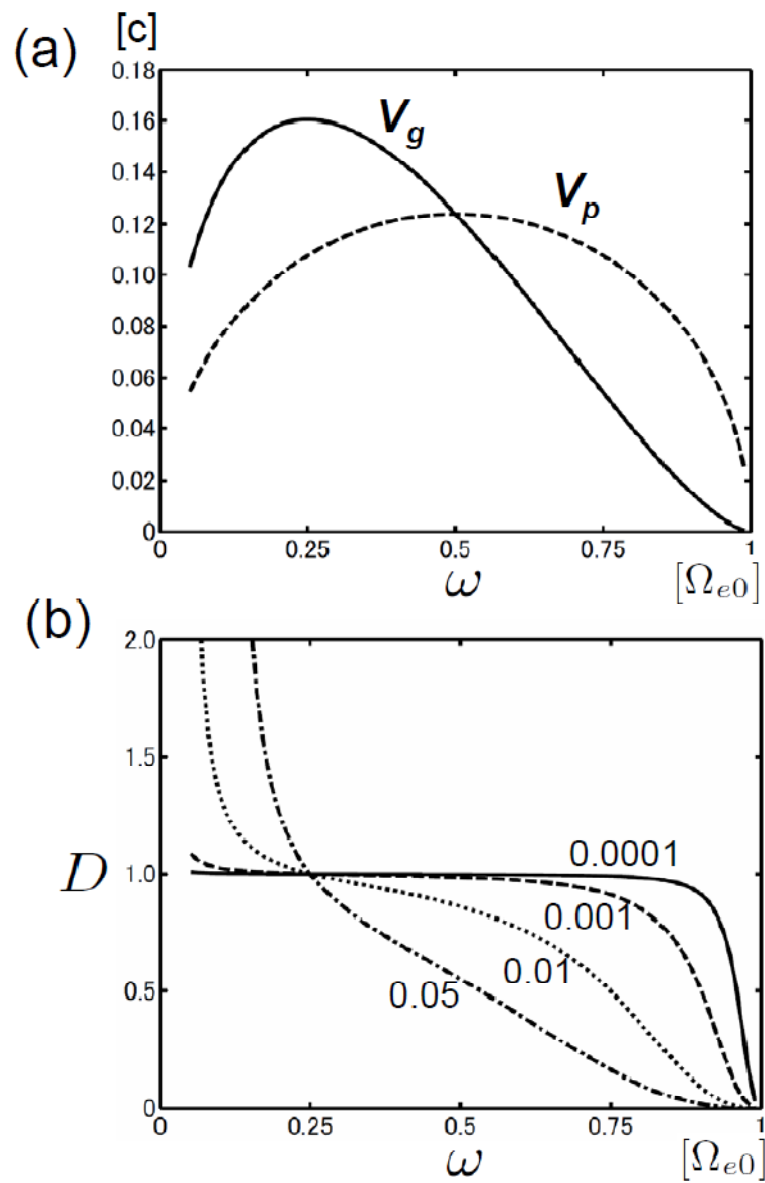


Figure 3. (a) The group velocity V_g and the phase velocity V_p as functions of frequency ω . (b) The frequency sweep rate factor for different values of $h_T(\partial\omega/\partial t)_{h=0}$ with $\omega_{pe}/\Omega_{e0} = 4$.

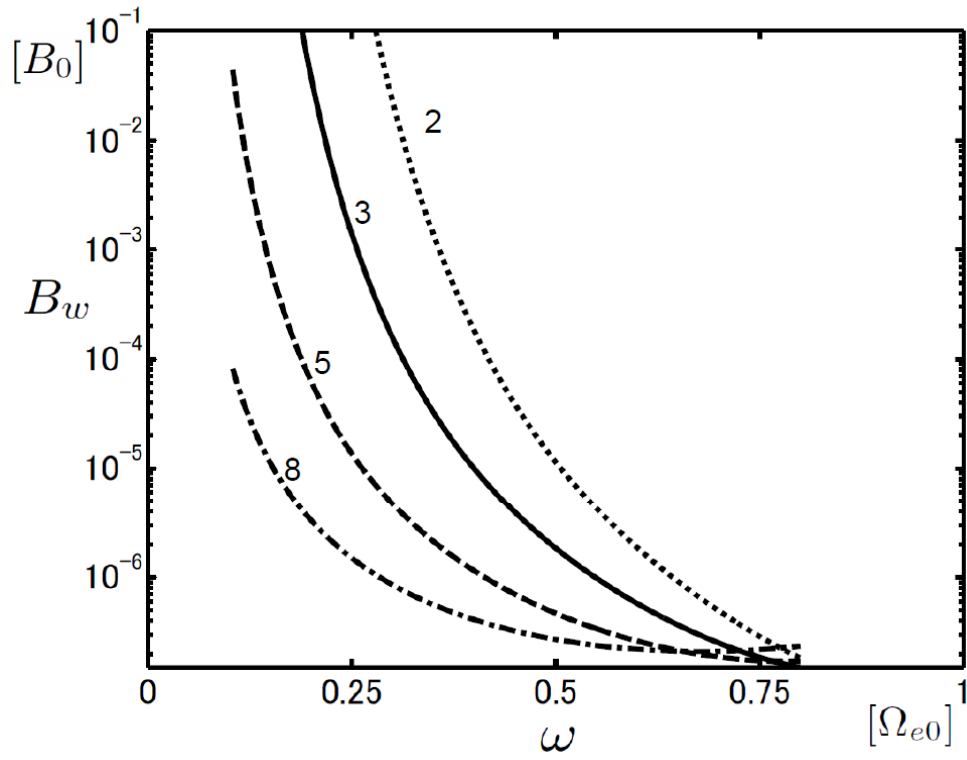
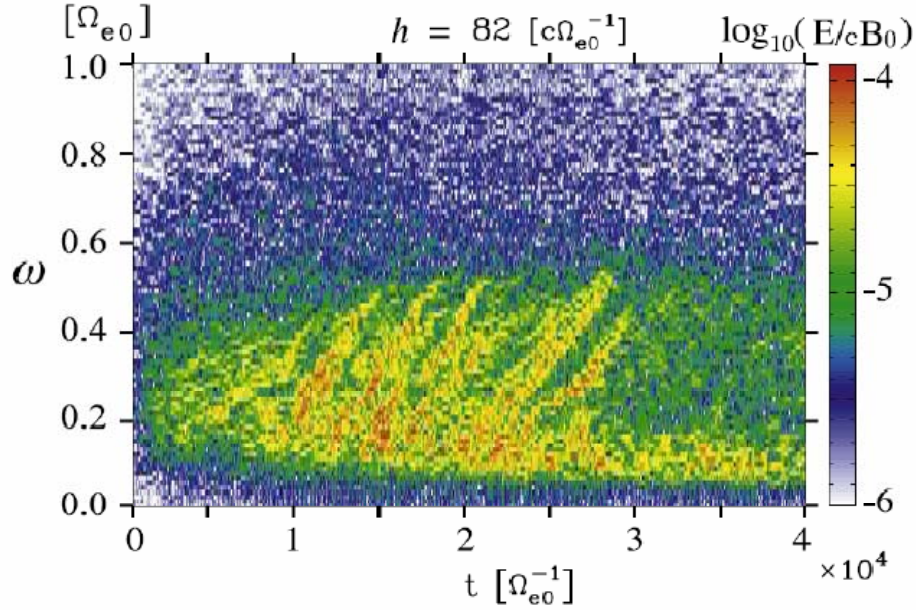


Figure 4. The wave amplitude threshold for the generation of self-sustaining chorus emissions for the plasma frequencies $\tilde{\omega}_{pe} = 2, 3, 5, 8$, (indicated by the attached numbers) and for the parameters $\tilde{U}_{t||} = 0.18$, $\tilde{V}_{\perp 0} = 0.21$, $\tilde{a} = 2 \times 10^{-7}$, $\tilde{\omega}_{ph} = 0.2$, and $Q = 0.5$.

(a) Simulation A



(b) Simulation B

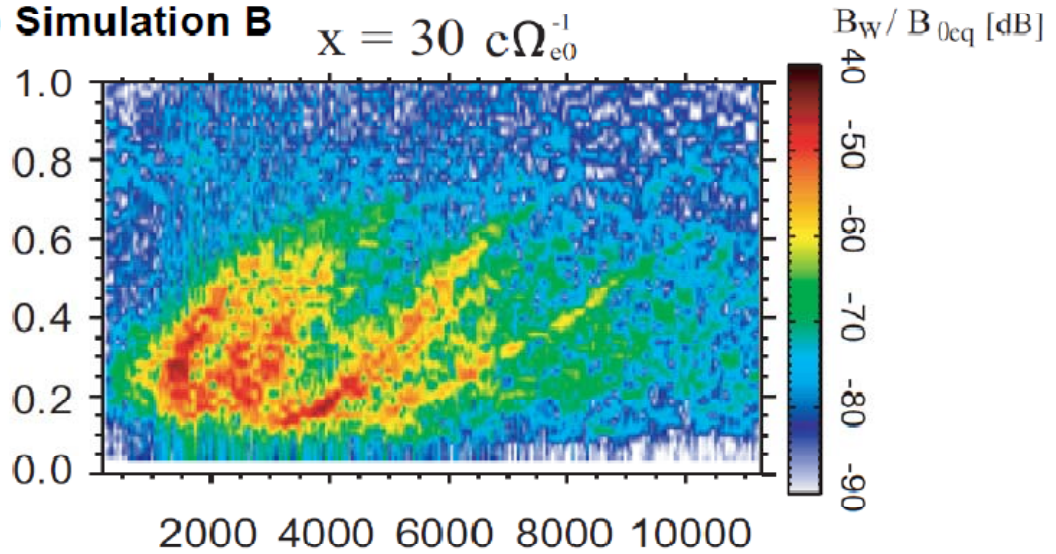
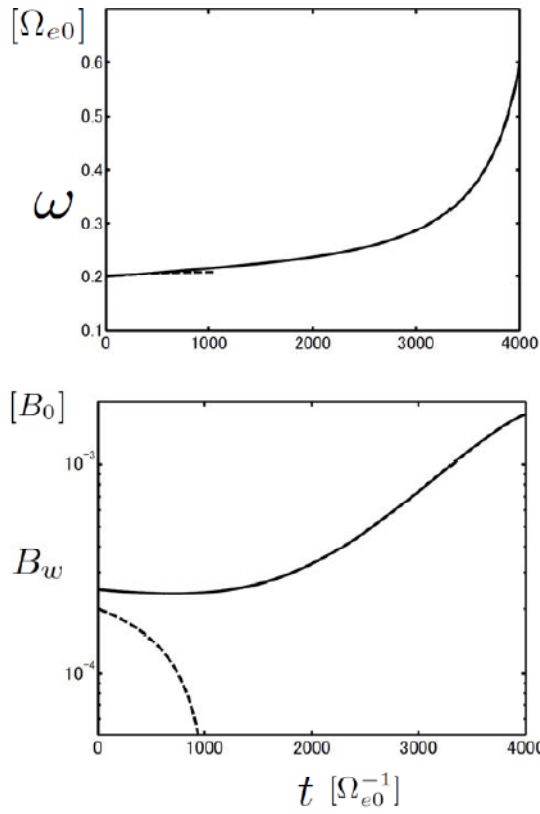


Figure 5. Dynamic spectra of the chorus elements reproduced by (a) Simulation A: the electron-hybrid code [after Omura *et al.*, 2008], and by (b) Simulation B: by the full-particle code [after Hikishima *et al.*, 2009].

(a) Simulation A



(b) Simulation B

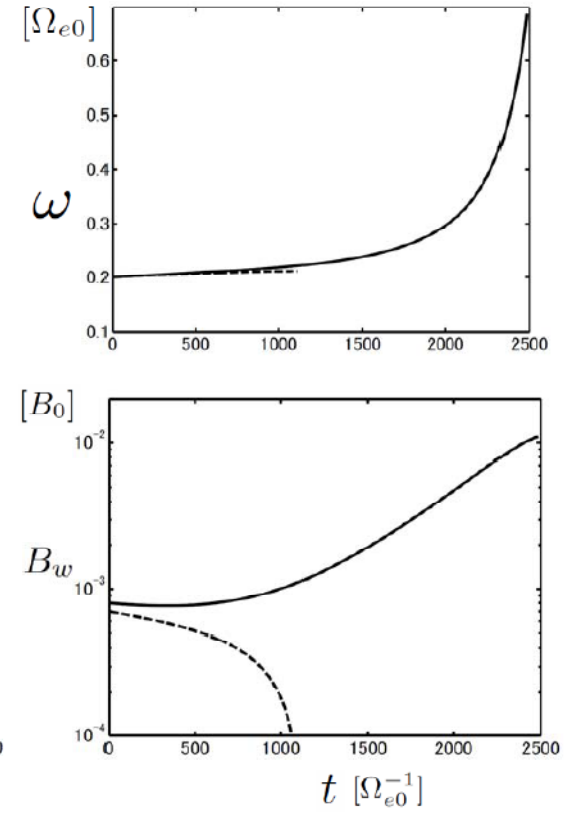


Figure 6. Solutions of the chorus equations for parameters used in (a) Simulation A and (b) Simulation B. The dashed line shows a solution below the amplitude threshold in each case.

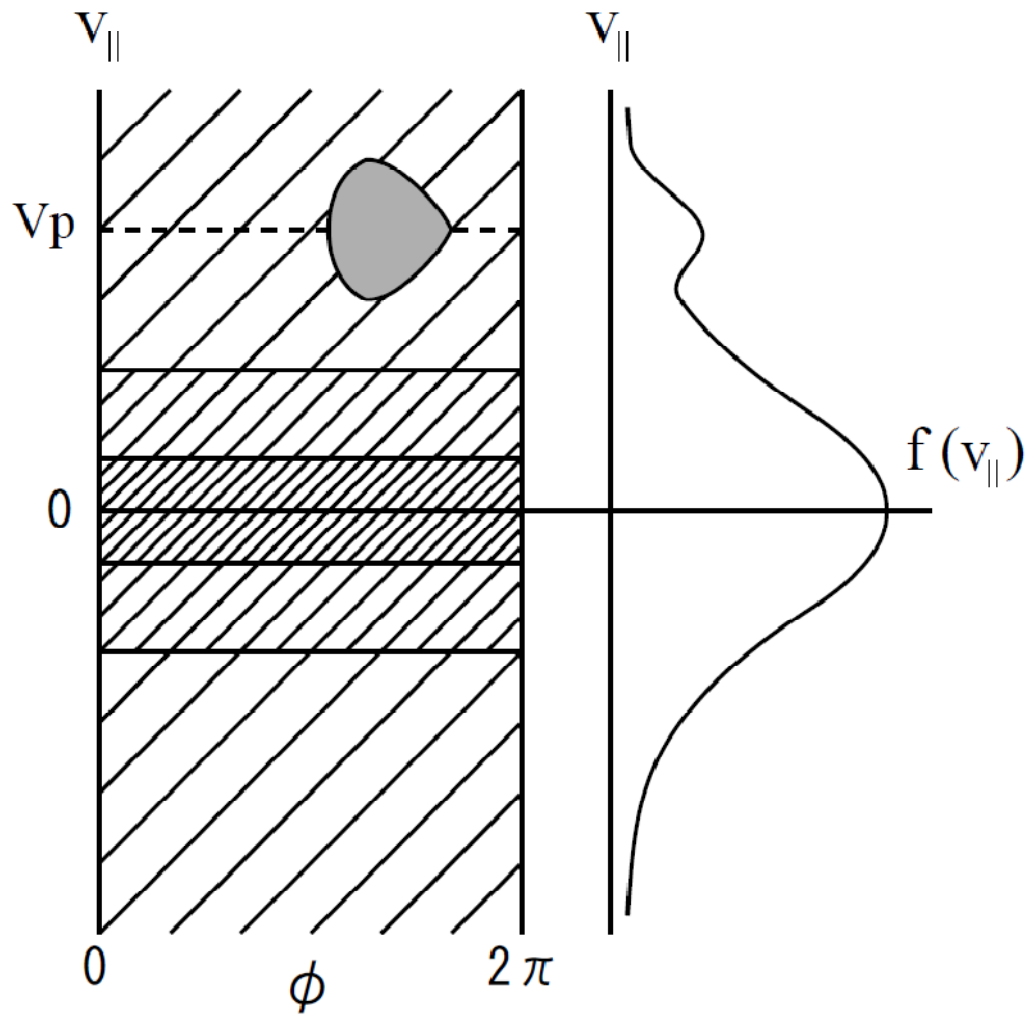
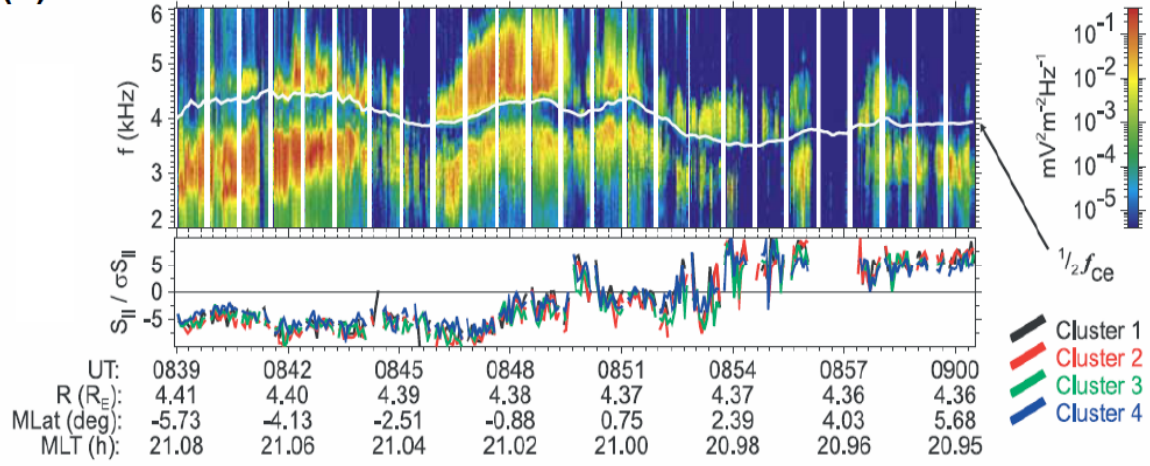


Figure 7. Schematic illustration of the distribution function of energetic electrons interacting with the longitudinal component of the whistler-mode wave packet propagating away from the magnetic equator.

(a) Earth



(b) Saturn

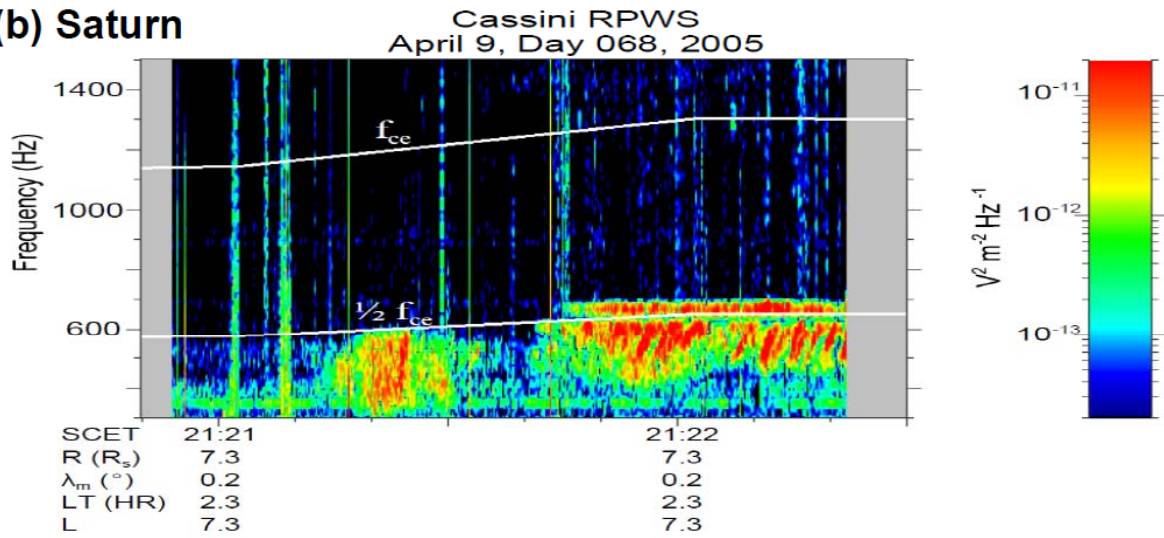


Figure 8. (a) Chorus emissions observed by the Cluster spacecraft in the Earth's magnetosphere ($L = 4.4$) [after Santolik *et al.*, 2003]. (b) Chorus emissions observed by the Cassini spacecraft in Saturn's magnetosphere ($L = 7.0$) [after Hospodarsky *et al.*, 2008].

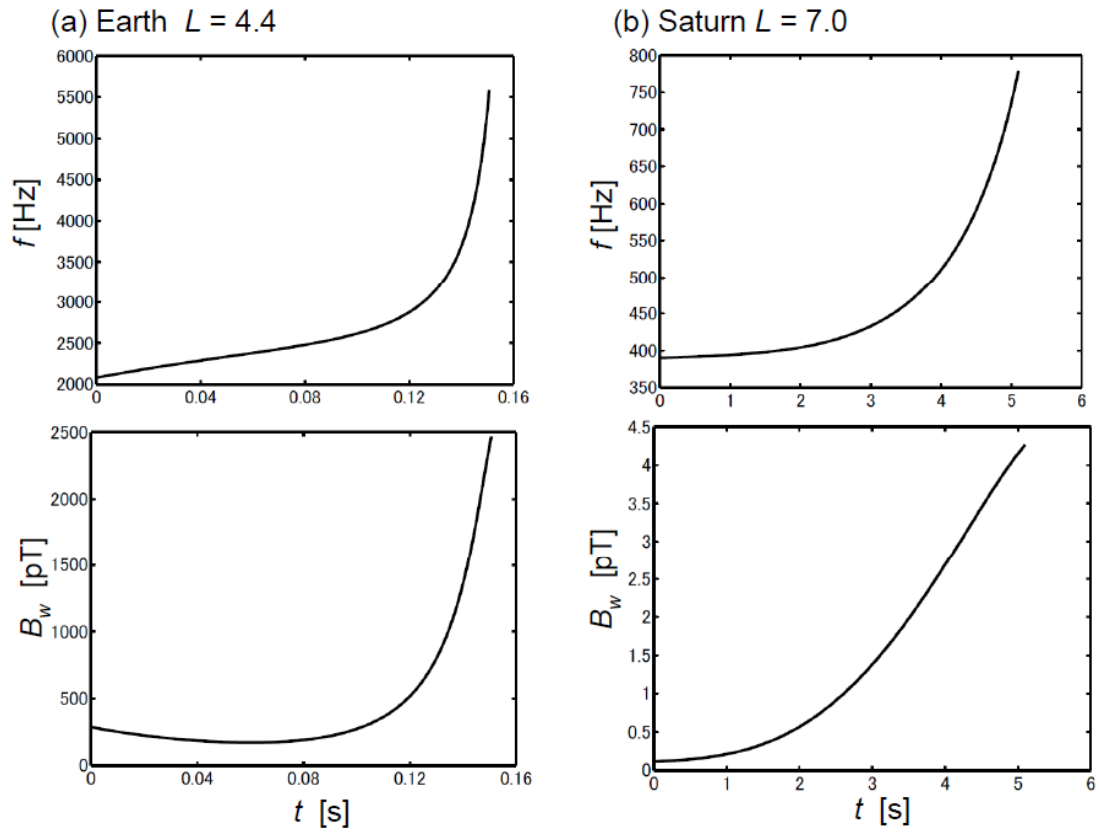


Figure 9. Solutions of the chorus equations (41) and (42) using parameters for (a) the Earth ($L = 4.4$) and (b) Saturn ($L = 7.0$).